2005

Quantification of Feline Immunodeficiency Virus (FIVpco) in peripheral blood mononuclear cells lymph nodes and plasma of naturally infected cougars

David B. Blake
The University of Montana

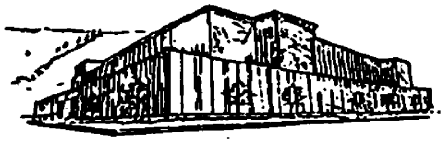

Quantification of Feline Immunodeficiency Virus (FIV_{pco}) in peripheral blood mononuclear cells, lymph nodes and plasma of naturally infected cougars

By

David Blake

B.A., University of Pennsylvania, Philadelphia Pennsylvania, 1999

Presented in partial fulfillment of the requirements

for the degree of

Master of Science

The University of Montana

December 2005

Approved by:

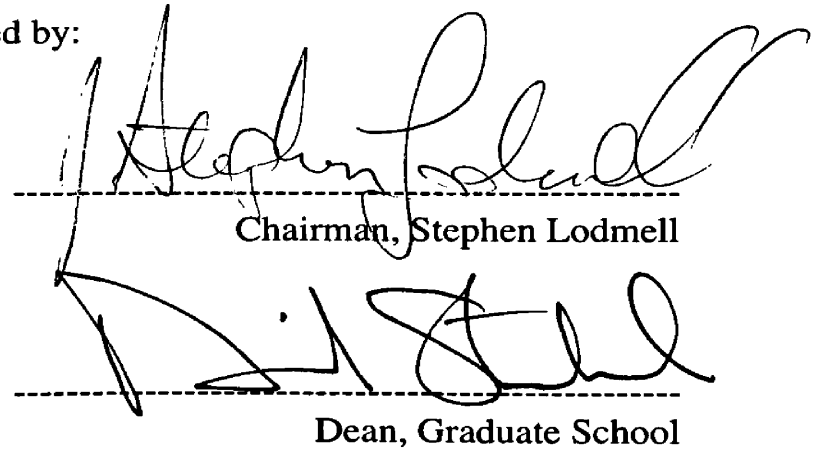

Chairman, Stephen Lodmell

Dean, Graduate School

10-18-05

Date

ProQuest LLC.
789 East Eisenhower Parkway
P.O. Box 1346
Ann Arbor, MI 48106 - 1346

Blake, David B., M.S. December 2005 Biochemistry

Quantification of Feline Immunodeficiency Virus (FIV_{pco}) in peripheral blood mononuclear cells, lymph nodes and plasma of naturally infected cougars

Chair: Stephen Lodmell

Infection of domestic cats with Feline Immunodeficiency Virus (FIV) results in a fatal immunodeficiency disease, similar to human immunodeficiency virus type-1 (HIV-1) in humans. Elevated plasma viral loads in domestic cats are correlated to decreased survival time and disease progression. FIV is also maintained as an apathogenic infection in other members of the family Felidae including cougars, *Puma concolor* (FIV_{pco}). It is not known whether the lack of disease in cougars is a result of diminished viral replication. A real-time PCR assay was developed to quantify both FIV_{pco} proviral and plasma viral loads in naturally infected cougars. Proviral loads quantified from peripheral blood mononuclear cells (PBMC) ranged from $2.90x10^1$ to $6.72x10^4$ copies per 10^6 cells. Plasma viral loads ranged from $2.30x10^3$ to $2.81x10^6$ RNA copies per ml. These data indicate that FIV_{pco} viral loads are comparable to viral loads observed in endemic primate lentivirus infections. Thus the lack of disease in cougars is not due to low levels of viral replication. Moreover, significant differences observed among cougar PBMC proviral loads correlated to viral lineage and cougar age ($P = 0.014$), which suggests that separate life strategies exist within FIV_{pco} lineages. This is the first study to demonstrate that an interaction of lentiviral lineage and host age significantly affects proviral loads.

Acknowledgements:

I want to thank Mary Poss for allowing me to work in her lab as well as my committee members, Stephen Lodmell, Scott Samuels, Mark Grimes and John Portis. Sally, Roman and Evan were all great to work with in the lab and I hope they continue to do good work. To all my fellow graduate students, Hennelly, Geo, Hector, Meghan and Nermi, good luck!

Table of Contents

Figures

Chapter 1

Chapter 2

Chapter 3

Chapter 1

Introduction

Introduction to lentiviral infections and disease

Lentiviruses are RNA viruses associated with the family *Retroviridae*. These viruses replicate their genomes through a reverse transcriptase enzyme and are frequently characterized by an extended incubation period prior to any evident signs of disease. For example, human immunodeficiency virus type-1 (HIV-1) infection in humans begins with an acute infection and over a period of years, progresses to immunodeficiency and ultimately death. While much attention has been paid to HIV-1 because of its enormous public health threat (Armstrong et al., 2005), lentiviruses infect a number of other animals such as sheep (visna virus), horses (equine infectious anemia virus), non-human primates (simian immunodeficiency virus (SIV)) and felines (feline immunodeficiency virus (FIV)) (Ligne, 1843, Lowenstine et al., 1986, Sigurdsson et al., 1952). Although many lentivirus infections are associated with disease, such as HIV-1 in humans and FIV in domestic cats, some lentivirus infections are endemic within wild populations and do not result in disease. For example, endemic lentivirus infections in African green monkeys (SIV_{agm}), sooty mangabeys (SIV_{sm}) and cougars (FIV_{pco}) results in no observable disease despite elevated viral loads (Holzammer et al., 2001, Olmsted et al., 1992, Rey-Cuille et al., 1998). Therefore, all lentivirus infections are not associated with pathogenic diseases.

Genomic organization of FIV

Feline immunodeficiency virus (FIV) is a lentivirus that infects members of the family Felidae worldwide. Although all FIV strains detected in wild and domestic cats form a monophyletic cluster in a phylogeny of lentiviruses, each feline species is infected with a distinct virus and infection results in disparate outcomes (Burkhard & Dean, 2003). FIV is maintained as an apathogenic infection in some members of the cat family such as lions (*Panthera leo*) and cougars (*Puma concolor)* (FIV_{pco}) (Brown et al., 1994, Carpenter & O'Brien, 1995, Olmsted et al., 1992). However, FIV infection in domestic cats results in a disease similar to HIV-1 in humans (Bendinelli et al., 1995, Pedersen et al., 1987).

The genome of FIV encodes three genes that are common to all retroviruses; *gag*, *pol* and *env*. *Gag* and *env* encode structural proteins that are necessary for virion assembly while *pol* encodes the enzymes needed for viral replication (Burkhard & Dean, 2003, Inoshima et al., 1998). Since FIV is a lentivirus, it also contains additional accessory genes that encode nonstructural proteins that alter viral gene expression and pathogenesis. One of these accessory genes, *rev*, is conserved across all lentiviruses and provides an essential mechanism by which partially and unspliced viral RNAs are exported from the nucleus (Miller et al., 2000). A transactivating gene is also encoded by all lentiviruses and plays an important role in viral transcription. The transactivating protein in FIV, Orf2, also facilitates transactivation but through a unique mechanism compared to transactivating proteins from other lentiviruses (Chatterji et al., 2002). *Vif* is also encoded by all lentiviruses except equine anemia virus and is necessary in HIV-1 infections to suppress a host-derived antiviral factor, APOBEC3G (Rose et al., 2004). FIV is genetically distinct from primate lentiviruses because it encodes a dUTPase gene

(Miller et al., 2000). dUTPase hydrolyzes dUTP into dUMP to maintain a low concentration of dUTP in the cell in order to reduce the opportunity of uracil misincorporation during reverse transcription. Finally, FIV does not encode accessory proteins such as *vpr*, *vpu* or *nef* as primate lentiviruses do.

Retroviral Life Cycle

Although FIV is phylogenetically distinct from other lentiviruses, the viral life cycles of all lentiviruses are similar and can be divided into six distinct steps that include entry, uncoating, integration, transcription, assembly and budding (Fig. 1.1). FIV utilizes CD134 as a primary receptor as well as the chemokine coreceptor, CXCR4 for attachment and entry (de Parseval et al., 2004a, de Parseval et al., 2004b, Shimojima et al., 2004). After attachment and membrane fusion the viral core, which includes the full-length genomic RNA and the viral reverse transcriptase (RT), is deposited into the cytoplasm. The viral genomic RNA is reverse transcribed by RT to form a full-length double stranded DNA copy. The double-stranded DNA then forms a preintegration complex with viral integrase (IN) and translocates to the nucleus. Integration of the viral DNA is catalyzed by IN and results in the random insertion of the viral DNA into the host genome. The integrated viral DNA form is called the provirus. After integration, transcription of the provirus by the host cell RNA polymerase II produces both full length genomic RNA as well as singly and fully spliced viral transcripts. These transcripts are subsequently translated into viral proteins such as Gag and Gag-Pol precursors, which are assembled into immature viral particles along with the full length genomic RNA. The assembled immature virions then bud from the host cell membrane. Mature virions are

produced after the viral protease (PR) cleaves the Gag and Gag-Pol precursors to form infectious viruses. Hence, lentiviruses exist as an integrated DNA provirus within an infected cell and as a cell free RNA virus circulating in the blood.

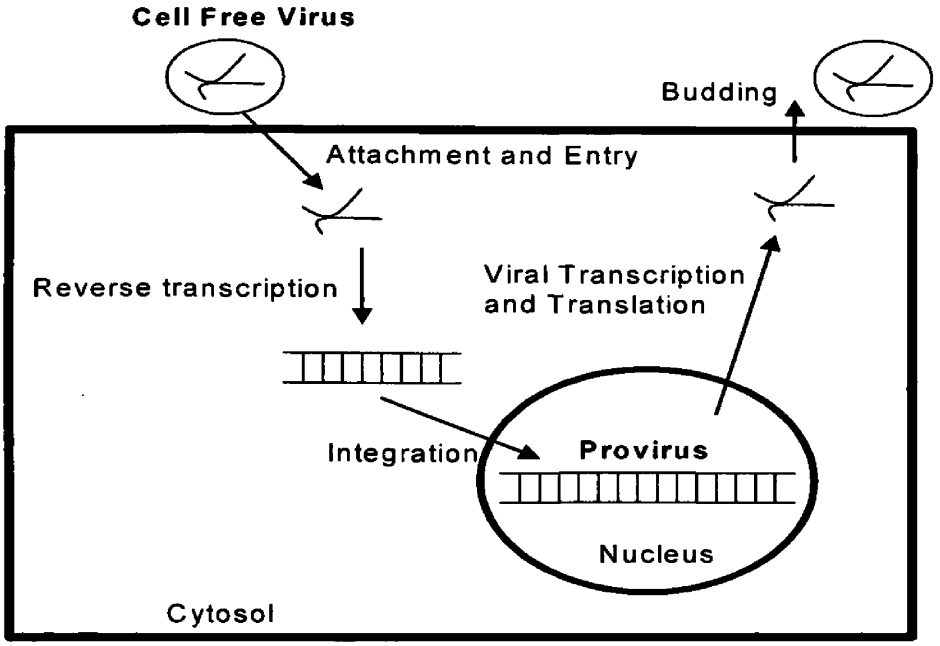

Figure 1.1: A schematic of the retroviral life cycle. Lentiviruses exist in both an RNA and DNA form during infection. Lentiviruses are present as infectious cell free virions, which contain the full length viral genomic RNA (indicated in red). After attachment and entry, the genomic RNA is reverse transcribed to double-stranded DNA (indicated in green) and integrated into the host cell genome (indicated in black), which is called the provirus.

Importance of viral loads on disease progression

Viral expression levels provide important information on the state of pathogenic lentivirus infections. In both HIV-1 and FIV infections, the acute stages of infection are associated with high plasma viral loads (Diehl et al., 1995, Piatak et al., 1993a, Piatak et al., 1993b). As the infection persists, viral RNA levels decrease and usually remain detectable throughout the infection. Viral RNA levels increase again in the terminal stage of the infection (Diehl et al., 1995, Gupta et al., 1993). Although viral expression levels increase during the beginning and end of pathogenic lentivirus infections, the amount of

cell free virus during the asymptomatic stage of the infection is the most robust prognostic indicator for disease progression and has been shown to correlate to survival times in FIV and HIV-1 (Diehl et al., 1996, Goto et al., 2002, Mellors et al., 1996).

Plasma viral loads have been shown to correlate to disease stage in both experimental and natural FIV infections in domestic cats. Domestic cats experimentally infected with FIV that progress rapidly to disease maintain plasma viral loads 1 to 2 logs higher than long-term survivors (Diehl et al., 1996). Moreover, the total amount of anti-FIV antibodies is not different between rapid disease progressors and long-term survivors indicating that FIV replication plays an important part in FIV disease progression. The premise that plasma viral loads are correlated to disease in FIV infections is also supported by observations from naturally infected domestic cats. High plasma viral loads ($\geq 10^6$ RNA copies per ml) in naturally infected domestic cats correlate to progression to feline AIDS as well as decreased survival times (Goto et al., 2002). Therefore, the amount of virus circulating in the blood of infected domestic cats provides a strong clinical marker for disease outcome and survival time during FIV infections.

Since elevated plasma viral loads are also correlated to disease progression in patients infected with HIV-1 (Mellors et al., 1996), patients currently receive highly active retroviral therapy (HAART), which enables them to remain free from clinical symptoms. HAART includes a combination of nucleoside and nonnucleoside inhibitors of the reverse transcriptase and protease enzymes that substantially inhibit the level of viral replication and decrease plasma viral loads to undetectable levels (Kulkosky & Pomerantz, 2002). Once plasma viral loads decrease to undetectable levels in patients (<50 copies per ml of blood), proviral loads become an important measure of efficacy of

antiretroviral therapy. The proviral reservoir is the major obstacle in the complete eradication of the virus. HAART therapy has been shown to also decrease HIV-1 proviral loads, however the rate at which HIV-1 proviral loads decrease are much lower than that of plasma viral loads (Dickover et al., 1992). Therefore, after prolonged HAART therapy, proviral loads provide a second clinical marker by which to compare the efficacies of different antiretroviral therapies (Desire et al., 2001, Dickover et al., 1992).

Viral loads in endemic apathogenic SIV infections

In contrast to pathogenic lentivirus infections in domestic cats and humans, primates infected with SIV maintain substantial viral loads but do not progress to disease. The amount of cell associated and cell free virus in infected African green monkeys (AGM) and sooty mangabeys (SM) indicates that these infected primates maintain viral loads equivalent or higher than viral loads in pathogenic lentivirus infections in domestic cats or humans despite remaining free from disease. For example, proviral loads quantified in three naturally infected sooty mangabey ranged from 2450 to 6020 DNA copies per 10^6 PBMCs, with a mean of $4.6x10^3$. Plasma viral loads quantified from these SM ranged from $4.7x10^5$ to $1.2x10^7$ RNA copies per ml (Rey-Cuille et al., 1998). In African green monkeys proviral loads were lower than in SM and ranged from 33 to 333 DNA copies per 10^6 PBMCs and 333 to 3333 DNA copies per 10^6 LN cells. However, plasma viral loads quantified from AGM in a separate study were similar in magnitude to SM (range $3.5x10^5$ to $>9.5 x10^6$ copies/ml) (Broussard et al., 2001). One study quantified plasma viral loads in six AGM ranging from less than 10^3 RNA copies per ml to $8x10^5$ (Goldstein et al., 2000). In a much larger study, viral loads in AGM ranged from $8.3x10^3$

to $1.1x10^7$, with a mean of $1.7x10^6$ RNA copies per ml (Holzammer et al., 2001). These data clearly indicate that naturally infected SM and AGM maintain a productive lentiviral infection despite remaining free from disease. Therefore, the amount of virus in an infected individual or animal is not always predictive of disease.

Quantification of viral loads

Since viral loads are frequently an informative measure of disease progression, several methods have been designed to quantify the amount of virus in an infected animal or patient. Competitive PCR is one method used to measure viral loads (Clementi et al., 1994, Orlando et al., 1998). In competitive PCR both the target and a truncated competitor are amplified simultaneously with the identical forward and reverse primer set. To insure that quantification through competitive PCR is accurate, the amplification efficiencies of both the target and competitor must be equal. When both templates amplify uniformly, the ratio of template and competitor will remain constant throughout the PCR. Therefore, to quantify the initial amount of target, an equal ratio of target to competitor must be identified through amplification and subsequent densitometry analysis. The initial amount of target is then calculated by determining the starting quantity of competitor used in that particular reaction.

Competitive PCR is labor intensive and necessitates much post-PCR analysis. Even before quantification begins, a DNA or RNA competitor must be created for every target of interest and that competitor must amplify with equal efficiency. Several dilutions must be tested to achieve a suitable ratio. Furthermore, the post-PCR quantification must be thorough and accurate to provide a correct estimation of the initial

target amount. After all these controls are completed, the initial amount of target can only be calculated to within a ten-fold difference of the competitor.

Competitive PCR has been previously used to measure feline proviral loads from several different tissues in domestic cats (Pistello et al., 1994). The number of FIV copies per microgram of genomic DNA was quantified by utilizing a fixed amount of cellular DNA and a known amount of competitor DNA with a 21 base pair deletion,. Interestingly, a dynamic range of proviral loads were quantified, ranging from 4300 copies in CNS tissue to as low as 10 copies per 10^6 cells in ovary tissue. However, since the target amplicon was larger the results may be skewed due to an increased amount of ethidium bromide being incorporated into the target amplicon compared to the competitor, which would produce inaccurate results (Pistello et al., 1994). A second group worked to eliminate this quantification problem by utilizing a fluorescent labeled second round PCR primer to create a more specifically labeled PCR product (Cammarota et al., 1996). However, a separate enzyme digestion was necessary after amplification, which created another possible variable in the quantification. Competitive PCR is labor intensive and does not always lead to repeatable, accurate results. Consequently, a more sensitive and accurate method of quantification has been developed.

Real-time PCR is a quantitative fluorescent-based PCR method that monitors the level of fluorescence during every cycle of a PCR reaction (i.e. in real-time) (Niesters, 2002). The fluorescent signal is proportionate to the amount of PCR product in the reaction and increases every cycle. Real-time PCR accurately quantifies the initial amount of target template by comparing the level of fluorescence of an unknown sample to the fluorescence of a known copy number standard. Quantification through real-time

PCR is quicker than competitive PCR methods because real-time PCR eliminates any post-PCR processing steps. More importantly real-time PCR is able to detect a number of target templates over a broad dynamic range thereby making quantification more accurate (Niesters, 2001).

A variety of different chemistries are currently available for real-time PCR assays. For example, Taqman chemistry utilizes a fluorogenic probe during PCR amplification that specifically hybridizes to the target sequence. Taqman probes are oligonucleotides slightly longer than the primers that contain a fluorescent reporter on the 5' end along with a quencher at the 3' end. When the probe is not bound to the target sequence and then irradiated during amplification, the fluorescent dye excites and its energy is transferred to the quencher producing no fluorescent signal. However, when the probe hybridizes to the target sequence, the reporter is cleaved by the 5' exonuclease activity of the Taq polymerase during the extension step of the PCR reaction. Cleavage and subsequent irradiation results in an increase in fluorescence. Since the probe only hybridizes with the target sequence, it is specific. Moreover, Taqman chemistry is able to detect down to a single copy of the target sequence in a given reaction. Therefore, because of its specificity and sensitivity, Taqman chemistry is the most popular real-time chemistry employed to date.

A less expensive alternative to Taqman chemistry is using real-time PCR with an intercalating DNA dye such as SYBR green. SYBR green dye is similar to ethidium bromide and fluoresces only when bound to double-stranded DNA. Although SYBR green is a cheaper option, a major difficulty with this chemistry is that the dye fluoresces when bound to any double-stranded DNA products, including non-specific products.

Consequently to accurately quantify copy number with SYBR green, it is essential to optimize the reactions and amplify only the target of interest. Although intercalating dyes are less specific, a quality control measure is available for this chemistry that is not available when using Taqman probes. A post-PCR melt curve analysis is a useful method to ensure a single PCR product is amplified with SYBR green. After amplification is complete, the temperature of the thermal cycler increases incrementally over time. As the temperature increases any double stranded DNA denatures, releasing the fluorophores, and thereby producing a spike of fluorescence. If only one PCR product accumulates then only a single peak will be observed in the melt curve analysis. However, if shorter PCR products are amplified such as primer-dimers two or more peaks will be visualized.

During real-time amplification the threshold cycle number (Ct) is the principal measure of fluorescence. The Ct is the cycle number at which a significant increase in fluorescence is first detected. The threshold cycle number is correlated to the exponential growth phase of PCR amplification. The Ct value is determined after a real-time PCR amplification and usually represents 10 times the fluorescent variance within the assay. The higher the initial amount of target within a reaction, the sooner the accumulated product will be detected producing a lower Ct value. Therefore, by amplifying a series of DNA standards of known copy number and plotting copy number versus Ct values, a linear standard curve is produced (Fig. 1.2). This curve can then be used to quantify unknowns within the same run.

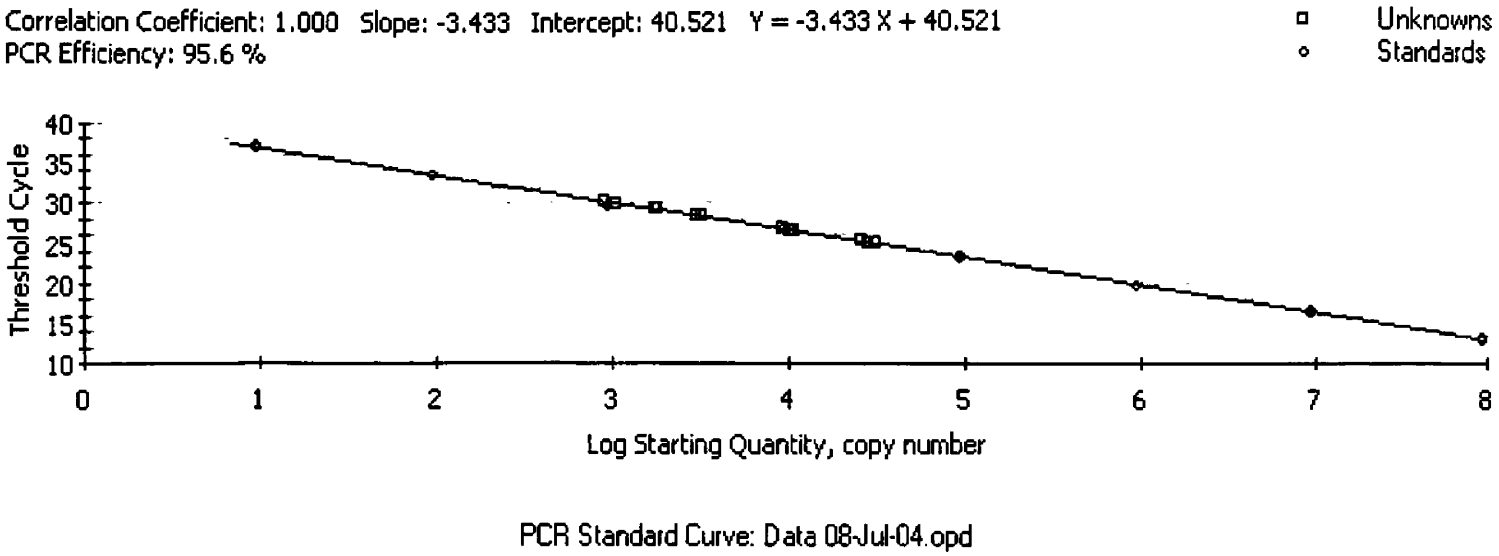

Figure 1.2: Quantification through real-time PCR. A series of myosin standards with a known number of copies were amplified through real-time PCR indicated by the blue circles. The numbers of standard copies (log quantity) are plotted against their respective threshold cycle values (Ct). The linear curve generated can then be used to estimate the initial copy number of unknowns that were amplified in parallel indicated by red squares.

Since real-time PCR enables a quick and reliable method by which to quantify the number of target copies in an unknown sample, we developed two novel real-time PCR assays to determine both the proviral and plasma viral loads in infected cougars using both Taqman and SYBR green chemistries. Although real-time PCR is a sensitive method of detection, the extensive divergence of FIV_{pco} may be a problem in accurately quantifying the amount of virus in infected cougars. The viral diversity observed in cougars is known to be larger than the diversity observed in domestic cats (Carpenter et al., 1996). Nucleotide mismatches within the primer binding site have been shown to result in disparate amplification efficiencies between standards and unknowns (Klein et al., 1999). Moreover, a difference in amplification efficiencies between standards and unknowns can dramatically affect quantification (Leutenegger et al., 1999). Therefore,

the real-time PCR protocol was optimized to ensure proper amplification and accurate quantification.

Because FIV is maintained as an endemic apathogenic infection in cougars, *Puma concolor* (FIV_{pco}), we hypothesized that the lack of disease in cougars may be a result of diminished viral replication. To test this hypothesis, a real-time PCR assay was developed to quantify FIV_{pco} proviral and plasma viral loads from infected cougars. The Specific Aims that were addressed in the research presented here:

Specific Aim 1: To develop a real-time PCR assay to quantify FIV_{pco} proviral and plasma viral loads.

Specific Aim 2: To quantify proviral and plasma viral loads from peripheral blood mononuclear cells (PBMC), lymph nodes (LN) and plasma of infected cougars

Chapter 2

Establishment of the FIV_{pco} proviral and plasma viral load real-time PCR assay

In order to develop a real-time PCR assay that accurately quantifies FIV_{pco} proviral loads in infected cougars, three main objectives must be accomplished. First, real-time primers must be designed to quantify both the number of cell equivalents and the number of FIV_{pco} provial copies. Then the optimal primer concentrations for each primer set must be established experimentally. Finally, the real-time assay must be designed so that the plasmid DNA standards and the genomic unknowns amplify with equivalent efficiencies. After these three objectives are completed proviral loads can be accurately quantified from cougar PBMC and LN samples.

Primer Design

Primer design for quantitative RT-PCR is typically accomplished through a computer program from Applied Bioscience Inc. (ABI) called Primer Express. This program accounts for certain variables that inhibit efficient real-time amplification by selecting primers and probes according to the following set of criteria. First, both the forward and reverse primer are designed to have a Tm, which is defined as the temperature at which 50 percent of the primer concentration is bound to the target sequence, of approximately 58 to 60°C. Additionally, the G-C content for each primer is designed to be between 20 and 80 percent and each primer does not have more than 40 percent of G's or C's at the 3' end. Finally, the size of the real-time PCR amplicon is limited to between 50 and 150 basepairs (bp) because smaller amplicons give more

consistent results and are more efficiently amplified in real-time. While designing the probe two major criteria are addressed. First, the 5' end of the probe must not include a guanine because this nucleoside base acts as a natural quencher during amplification. Second the number of G's cannot be greater than the number of C's.

Proviral loads are typically calculated based upon the number of viral DNA copies per million cell equivalents (Damond et al., 2001, Desire et al., 2001). Therefore, to quantify FIV_{pco} proviral loads from infected cougar PBMC and LN, the number of cell equivalents and the number of FIV_{pco} proviral copies must be determined for each genomic sample. In this assay a portion of exon 19 of the cougar myosin gene was selected as our determinant for the number of cell equivalents. Since this gene is well conserved in cougars, a Taqman primer and probe set was created that was 100% complementary to the myosin sequence. However, to quantify FIV_{pco} copy number, no suitable Taqman probe could be designed because of the extensive sequence divergence within FIV_{pco}. Previous FIV_{pco} phylogenetic studies have established that distinct viral lineages of FIV_{pco} exist within cougar populations in western North America and that the genetic diversity among cougar lentiviral lineages is greater than the diversity observed in FIV in domestic cats (Biek et al., 2003, Carpenter et al., 1996). Therefore, SYBR green chemistry was used for the quantification of FIV_{pco}. The FIV_{pco} primer set targeted a conserved region located at the 3' end of the putative *env* gene, which amplified a 170 bp fragment.

Construction of plasmid DNA standards

After the myosin and FIV_{pco} primer sets were identified through Primer Express, DNA plasmid standards were created for both myosin and FIV_{pco}. In the case of myosin, genomic cougar DNA was PCR amplified using the real-time myosin primers. For the FIV_{pco} DNA standards, cougar genomic DNA was amplified from five separate cougars that represented all FIV_{pco} viral lineages. The PCR products for both myosin and FIV_{pco} were subject to gel electrophoresis, gel purified, ligated into the pDrive vector and cloned (see Materials and Methods, Chapter 3). Plasmid DNA was purified and quantified through UV spectroscopy. To determine the number of copies for each DNA standard the following equations were used:

1) (bp size of double-stranded product)(330 daltons x 2 nt/bp) = **X** daltons, (daltons = grams/mole)
2) (**X** grams/mole) / (6.023×10^{23} molecules/mole) = **X** grams/molecule
3) Plasmid concentration (g/μl) / **X** grams/molecule = # of molecules of plasmid/μl

Rationale behind primer concentration optimization

Real-time PCR primer concentrations usually range from 50 to 900 nM. Therefore the optimal primer concentrations can be easily determined by independently varying the forward and reverse primer concentrations with a primer matrix as seen in Table 2.1. The primer concentrations that provide the optimal amplification are concentrations that yield the lowest threshold cycle number (Ct) and that produce no primer dimers. Primer dimer formation is unwanted in real-time PCR reactions because they are non-specific products and produce inaccurate results during quantification. Primer dimer formation can frequently be overcome by using unequal forward and reverse primer concentrations in the PCR reaction.

During any real-time primer optimization it is recommended that all amplifications are done with SYBR green because of two factors. First, SYBR green is a more economical choice during optimization than the Taqman probe. Second, with SYBR green a post-PCR melt curve analysis can be done for all reactions to determine whether any primer dimer formation has occurred. Non-specific products are of major concern while using SYBR green chemistry because any nonspecific double stranded DNA products bind the intercalating dye and fluoresce during the PCR reaction. However, with Taqman chemistry the probe is created to specifically hybridize to the target sequence and therefore nonspecific products are not amplified. After the optimal primer concentrations have been established, the amount of Taqman probe used for each reaction can be optimized. Probe concentrations usually range from 50 to 250 nM per reaction. Again the optimal probe concentration is the concentration that results in the lowest Ct value.

Optimization of the myosin primers and probe

For the myosin primer optimization, a primer matrix (Table 2.1) was prepared and amplified with SYBR green with a single myosin standard at a concentration of $8x10^5$ copies per reaction. All reactions amplified (Fig. 2.1) and only a single peak was observed in the melt curve analysis (data not shown). The reactions that included the highest forward and/or reverse primer concentrations (900nM) produced the lowest Ct values, indicating that higher primer concentrations increased the robustness of the real-time reactions. However, in a separate amplification reaction, using four different myosin primer concentrations and cougar genomic DNA (1.0 ug) as a template, the primer

concentrations of 300nM forward and 100nM reverse produced the lowest Ct value (Fig. 2.2). All standards and genomic samples were run in duplicate and the average Ct values from the duplicate reactions were calculated to determine the threshold cycle number. Since the cougar myosin gene was to be quantified from genomic cougar DNA, it was sensible to choose the primer concentrations (300F/100R) that amplified the genomic cougar DNA more efficiently.

To determine the optimal myosin probe concentration, two separate plasmid DNA standards ($8x10^5$ and $8x10^2$ copies per reaction) were amplified with the optimal myosin primer concentration (300F/100R) along with three different concentrations of the myosin probe (50, 100, and 250nM per reaction). The Ct values obtained among all three probe concentrations for each plasmid DNA standard were not significantly different (data not shown). Therefore, the probe concentration was chosen to be 50nM per reaction.

Table 2.1: Primer Optimization Matrix

	Forward Primer (nM)		
Reverse Primer (nM)	**100**	**300**	**900**
100	100 / 100	100 / 300	100 / 900
300	300 / 100	300 / 300	300 / 900
900	900 / 100	900 / 300	900 / 900

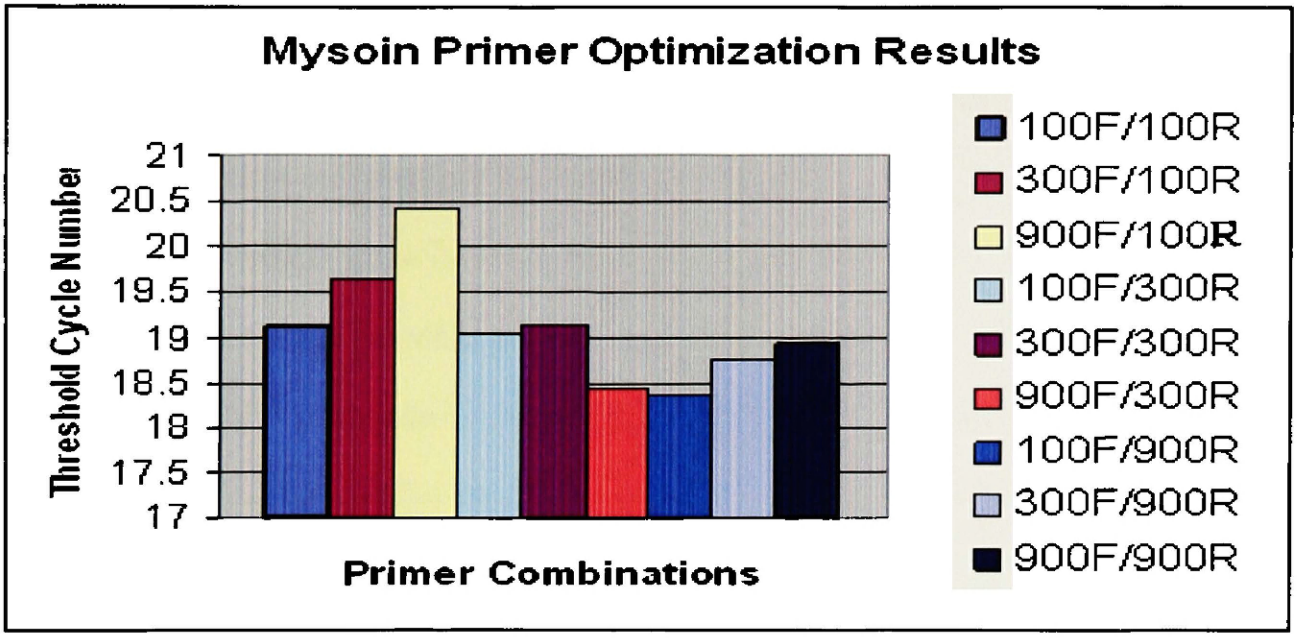

Figure 2.1: Optimization of the myosin primer concentrations. A single myosin DNA plasmid standard ($8x10^5$ copies/reaction) was amplified through real-time PCR with different concentrations of both forward and reverse myosin primer indicated in the legend.

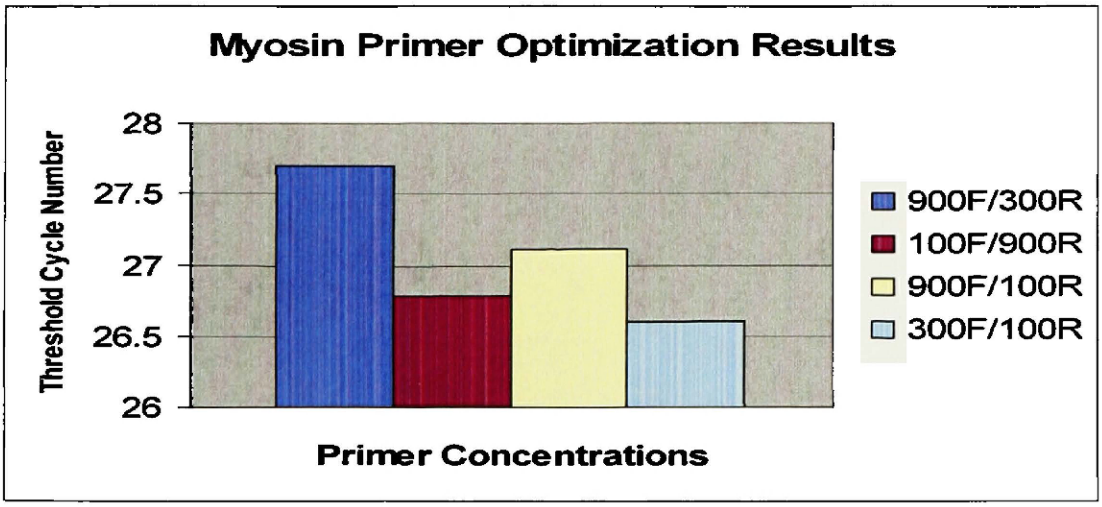

Figure 2.2: Optimization of the myosin primer concentrations using cougar genomic DNA. 1 ug of cougar genomic DNA was amplified through real-time PCR with four myosin primer concentrations indicated in the legend. The four myosin primer concentrations amplified the myosin plasmid DNA standards with different efficiencies.

Optimization results of FIV_{pco} primer set

To determine the optimal primer concentrations for the FIV_{pco} primers, an identical primer matrix was amplified with a single FIV_{pco} standard of $4x10^6$ FIV_{pco} copies per reaction utilizing SYBR green chemistry (Fig. 2.3). All reactions amplified and produced a single peak in the melt curve analysis (data not shown). The primer matrix identified three possible primer concentrations that most efficiently amplified the FIV_{pco} plasmid DNA standard; 300F/300R, 100F/900R, 900F/900R. Because these three primer concentrations produced Ct values that were within two cycle numbers of each other and taking into account the amount of primer used in each reaction, the primer concentration of 300nM forward and 300nM reverse was subsequently chosen as the optimal FIV_{pco} concentration.

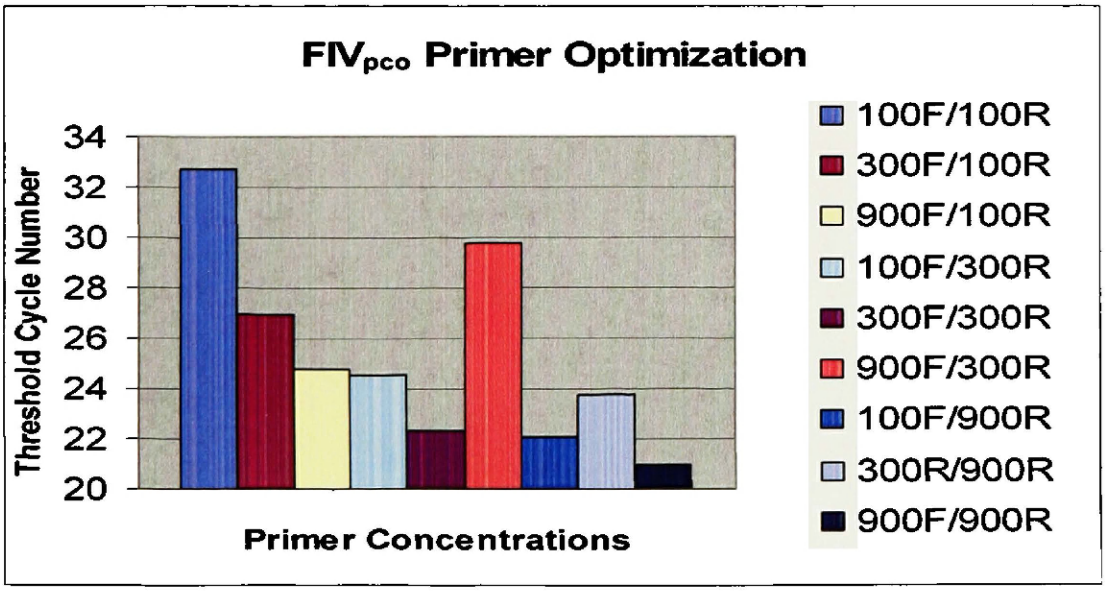

Figure 2.3: Optimization of the FIV_{pco} primer concentrations. A single FIV_{pco} DNA plasmid standard ($4x10^6$ copies per reaction) was amplified through real-time PCR with different concentrations of both forward and reverse FIV_{pco} primer indicated in the legend.

Investigating the accuracy of the real-time PCR quantification with the optimized myosin primer and probe concentrations

Although both primer sets amplified a single PCR product, the accuracy of the real-time assay needed to be determined. To this end, the myosin plasmid DNA standards were amplified in parallel to a series of known genomic cougar DNA concentrations to quantify the number of cell equivalents. Given that an animal cell contains 2 copies of DNA per cell and that animal genomic DNA weighs about approximately $1.9*10^{12}$ daltons, a single cell contains six picograms of DNA (Sambrook, 1989). Therefore, the theoretical number of cougar cells within each reaction was calculated. The theoretical number of cougar cells was then compared to the number of cell equivalents quantified by the myosin real-time PCR assay (Table 2.2). We assumed that a single cell contains two copies of a gene, therefore, the number of cell equivalents per reaction was calculated by dividing the number of myosin copies quantified by real-time PCR by a factor of two. The number of cells was also enumerated prior to DNA purification, which supported the number of theoretical cougar cells.

Table 2.2: Comparison of the number of cell equivalents quantified theoretically and through the myosin real-time PCR assay.

Concentration of cougar genomic DNA (ng/reaction)	Number of cell equivalents at 6 pg/ul (cells/reaction)	Number of cell equivalents from real-time quantification (cells/reaction)	Fold difference between real-time and theoretical cell quantification
$2.855x10^{3}$	$4.76x10^{5}$	$2.33\ x10^{5}$	~ 2
$2.855x10^{1}$	$4.76x10^{3}$	$4.26\ x10^{4}$	8.9
$2.855x10^{-1}$	$4.76x10^{1}$	$2.04\ x10^{2}$	4.3
$2.855x10^{-2}$	5.0	$2.3\ x10^{1}$	4.6

The results, which are summarized in Table 2.2, clearly indicate the numbers of cell equivalents in the three most dilute samples were all overestimated by more than a factor of 4. However, the most concentrated sample (> 2.0 μg/reaction) did estimate the

number of cell equivalents correctly. These results suggested that either the assay was optimized and DNA was lost or degraded in the most dilute samples prior to quantification or that the assay was not optimized and the most concentrated sample did not amplify efficiently.

Real-time quantification is known to be accurate between 0.1 and 1.0 μg of DNA per reaction (ABI technical bulletin #4304449C), which suggests that the most concentrated sample contained an excess amount of DNA in the PCR reaction that inhibited real-time amplification. Moreover, additional experimental data indicated that when enumerating more than 10^5 cell equivalents per reaction, amplification is not as efficient compared to genomic samples with less than 10^5 cell equivalents per reaction (data not shown). Therefore, the most concentrated sample did not amplify properly indicating the quantification of cell equivalents was incorrect based on the myosin standard curve and further optimization was necessary.

Since the quantification of cell equivalents is based upon the myosin standard curve, the inaccurate quantification may be due to unequal amplification efficiencies between the DNA plasmid standards and the genomic unknowns. Therefore, the effect of carrier DNA and conformation of the plasmid DNA standards on real-time amplification was investigated.

Investigating the effect of carrier DNA on real-time amplification

The effect of carrier DNA on real-time amplification was previously described in a real-time PCR assay that quantified FIV proviral loads in domestic cats (Leutenegger et al., 1999). This study determined that the Ct values of DNA plasmid standards decreased,

on average 0.5 cycle numbers, with the addition of carrier DNA. Moreover, the optimal carrier DNA concentration was determined to be 30 ng/reaction. Therefore, we investigated whether carrier DNA had an effect on the amplification of the myosin plasmid DNA standards.

To this end, a series of myosin DNA plasmid standards were serially diluted in the presence of either no carrier DNA, carrier DNA at a final concentration of 3 ng/reaction or carrier DNA at a final concentration of 30 ng/reaction. The three standard curves were subsequently amplified simultaneously through real-time PCR (Fig.2.4). The results indicated that the Ct values of all myosin plasmid DNA standards decreased approximately 5 cycles with the addition of carrier DNA at a final concentration of 30 ng/reaction. Moreover, the influence of carrier DNA on Ct values was greater in the DNA plasmid standards with the fewest number of copies, which is to be expected due to reduced amount of DNA in these low copy number standards. Carrier DNA alone did not amplify above threshold indicating the primer set was specific for myosin. The addition of carrier DNA to the DNA plasmid standards was therefore included in our assay and the optimal concentration of carrier was established to be 30 ng/ul.

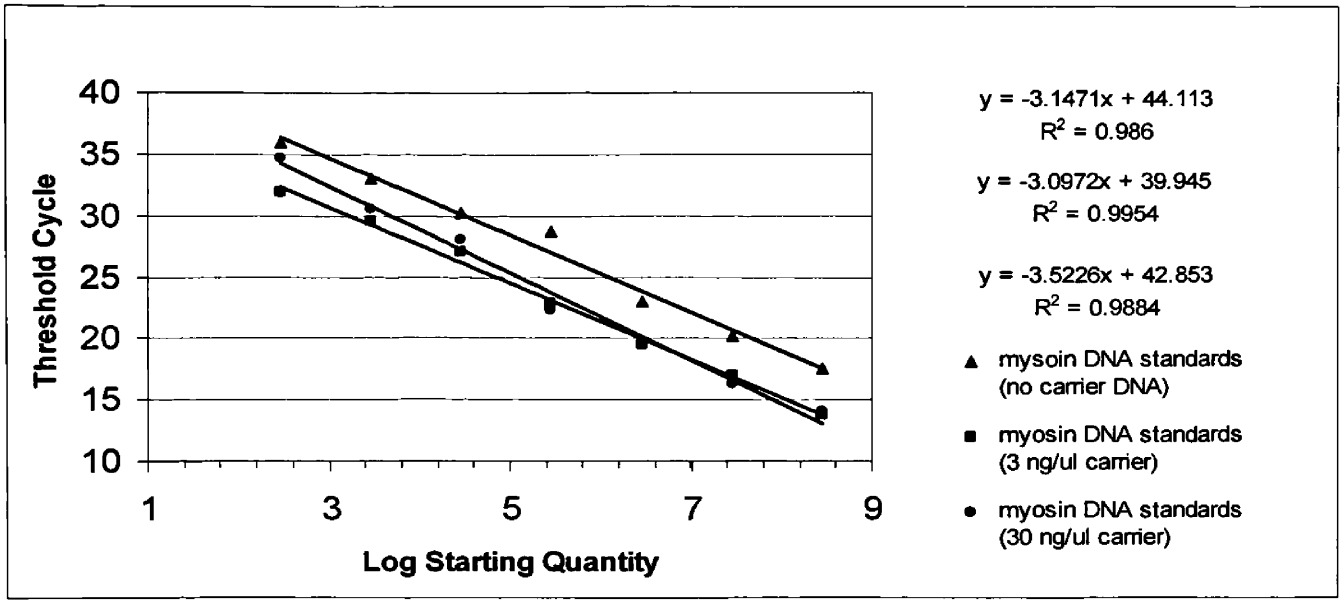

Figure 2.4: Effect of carrier DNA on real-time PCR amplification. Three separate myosin standard curves, containing either 0, 3 or 30 nanograms of carrier DNA per reaction, were evaluated simultaneously through real-time PCR. Each data point represents the average value of duplicate reactions.

Investigating the effect of linearizing plasmid DNA standards on real-time amplification

Since the addition of carrier DNA influenced the amplification of the DNA plasmid standards and the standards must amplify with equivalent efficiency in order to accurately quantify a sample, it follows that the environment of the standards within the PCR reaction should mimic the environment of the unknowns. Given that cougar genomic DNA is linear and the plasmid DNA standards are circular, the amplification efficiencies of the circular standards and genomic unknowns may be different. We therefore investigated the differences in Ct values between linearized and circular myosin DNA plasmid standards and the effect on quantifying the number of cell equivalents.

To understand the influence of DNA conformation on amplification, plasmid DNA containing the myosin insert was linearized through a restriction digest with Xho I that cleaves the vector at a single site. The linearized DNA was then purified with the

QIAquick PCR Purification Kit (Qiagen) and serially diluted (see Materials and Methods, Chapter 3). Circular and linear myosin DNA plasmid standards were amplified in parallel both containing carrier DNA at a final concentration of 30 ng/ul (Fig. 2.5). In addition, serial dilutions of cougar genomic DNA was quantified with both set of standards.

The results indicated that the threshold cycle values were dramatically lower with linear DNA plasmid standards compared to the circular standards, suggesting that the linear DNA standards amplified more robustly (Fig. 2.5). The number of theoretical cell equivalents (approximated at 6 pg/cell) was more appropriately quantified by the linear DNA plasmid standards, which exhibited only a 2-fold difference in the number of cell equivalents between the theoretical and real-time calculations (Table 2.3). The circular standards again overestimated the number of cell equivalents by a factor of ten. Consequently, all DNA plasmid standards were linearized prior to real-time amplification.

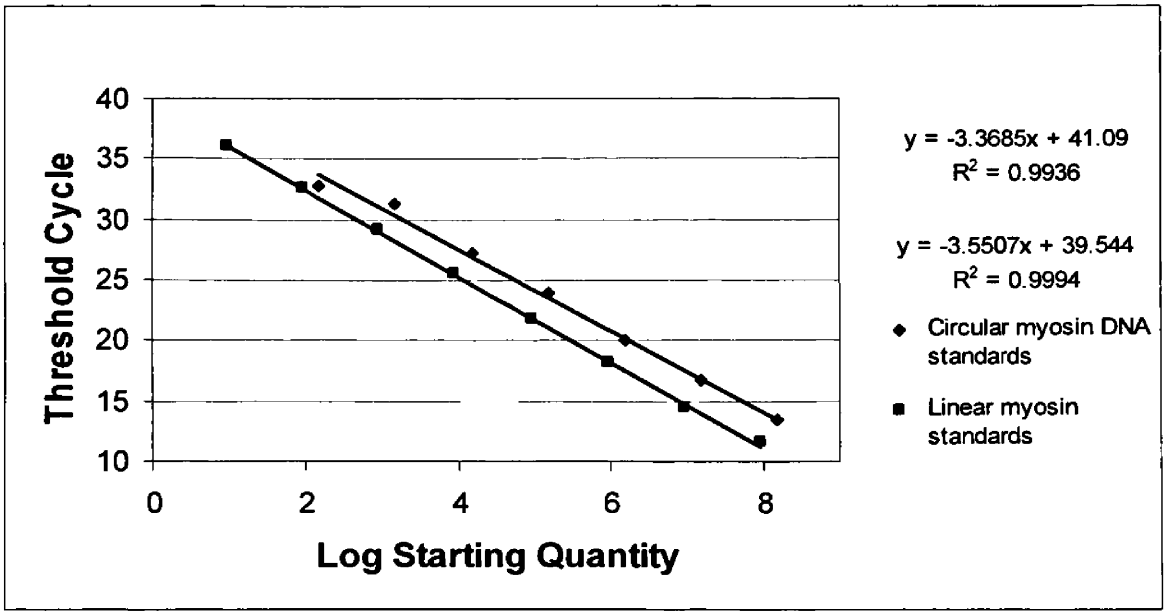

Figure 2.5: Amplification of circular and linear DNA plasmid standard curves. Two separate myosin standard curves, containing either circular or linear DNA plasmid standards, were amplified simultaneously through real-time PCR. Each data point represents the average value of duplicate reactions.

Table 2.3: Variation in quantifying the number of cell equivalents by using circular and linear DNA plasmid standards during real-time PCR.

Concentration of cougar genomic DNA (ng/reaction)	Theoretical number of cell equivalents at 6 pg/ul (cells/reaction)	Number of cell equivalents quantified with circular plasmids (cells/reaction)	Number of cell equivalents quantified with linear plasmids (cells/reaction)
$2.855x10^{3}$	$4.76x10^{5}$	$1.35x10^{5}$	$2.94x10^{4}$
$1.43x10^{2}$	$2.38x10^{4}$	$1.98x10^{5}$	$4.19x10^{4}$
$7.14x10^{0}$	$1.20x10^{3}$	$1.07x10^{4}$	$2.61x10^{3}$
$3.57x10^{-1}$	$5.95x10^{1}$	$3.95x10^{2}$	$1.15x10^{2}$

Comparison of amplification efficiencies between plasmid DNA standards and genomic unknowns

Finally to accurately quantify the number of DNA copies in an unknown sample, the amplification efficiency of the standards and unknowns must be equivalent. To determine whether the standards and unknowns amplify in the same way, the efficiency of the reaction must be calculated. The efficiency of a reaction is defined as $10^{-1/slope}$ and identifies the number of PCR products made during each cycle. To determine if amplification of the plasmid standards and genomic DNA was equivalent, the myosin standard curve was compared to a 10-fold dilution series of cougar genomic DNA that spanned the range of genomic DNA concentrations used to estimate the number of cell equivalents (Fig. 2.6). The efficiencies (defined as $10^{-1/slope}$) of the plasmid and genomic samples were 1.90 and 1.91 respectively, indicating that plasmid and genomic DNA amplified with equivalent efficiency in our assay.

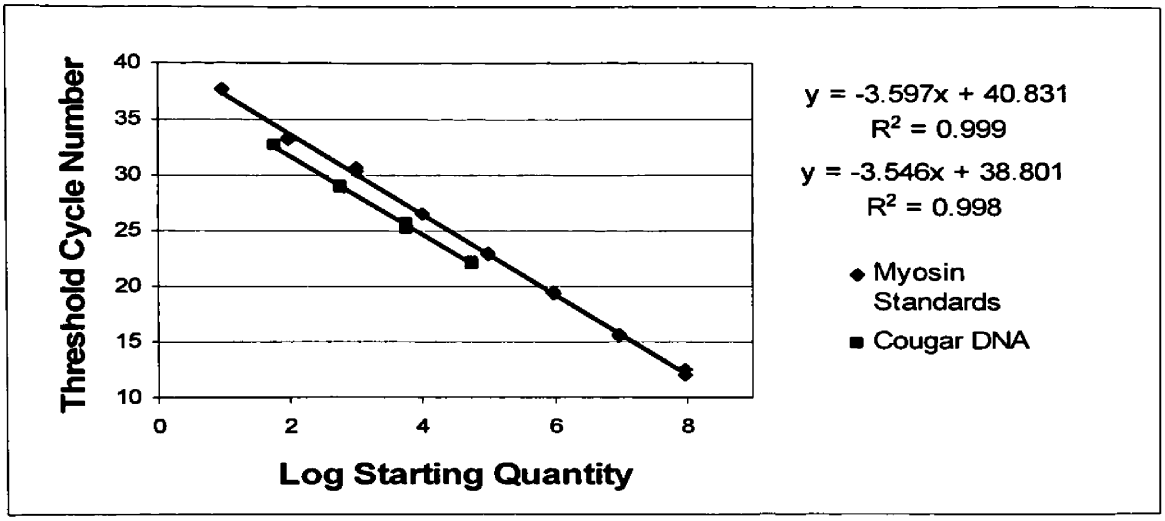

Figure 2.6: Efficiency comparison between myosin plasmid DNA standards and cougar genomic DNA. A series of ten fold dilutions of genomic cougar DNA was amplified in parallel to the myosin plasmid DNA standards to determine whether amplification efficiencies were equal. Efficiency is defined as $10^{-1/slope}$.

Optimization of the FIV_{pco} plasma viral load real-time PCR assay

FIV_{pco} exists as a cell free RNA virus in the blood. Therefore, to properly quantify plasma viral loads in infected cougars, an additional reverse transcriptase (RT) step was required in the existing FIV_{pco} real-time assay. The RT step necessitated the production of RNA standards and confirmation that the RNA standards and unknowns amplified with equivalent efficiencies.

Viral genomic RNA was obtained by isolating viral particles from the supernatant of a coculture of infected cougar PBMC. Viral genomic RNA was subsequently purified and incubated with DNase to degrade any contaminating genomic DNA (see Materials and Methods, Chapter 3). Viral genomic RNA was quantified through UV spectrophotometry and the number of genomic RNA copies was determined through the equation below:

1) (base size of full length genomic RNA (estimated at 9400b))(340 daltons) = 3.196×10^6 daltons, (daltons = grams/mole)

2) $(3.196 \times 10^{6}$ grams/mole) / $(6.023 \times 10^{23}$ molecules/mole) = 5.31^{-18} grams/molecule
3) RNA concentration (g/μl) / 5.31^{-18} grams/molecule = number of RNA molecules/μl

After the number of genomic RNA copies per microliter was determined, RNA standards were created through a series of serial dilutions in DEPC-treated water.

Investigating the effect of carrier RNA on RT real-time amplification

The effect of carrier RNA on the amplification in the RT real-time assay was then investigated because of two factors. First, carrier DNA dramatically influenced the real-time amplification in the FIV_{pco} proviral assay, indicating that the addition of carrier played an important role in the real-time PCR assay (see above). Second, viral RNA purified from the plasma of infected cougars is eluted in DEPC-treated water containing carrier tRNA (Sigma) at a final concentration of 63 ng/μl to aid in recovery. Therefore, carrier RNA was added to the RNA standards to equalize the RNA concentrations between standards and unknowns. To determine whether exogenous RNA had an effect on amplification, two separate RNA standard curves were amplified in parrallel. One RNA standard curve included no carrier RNA and the other RNA standard included carrier RNA at a final concentration of 63 ng/μl.

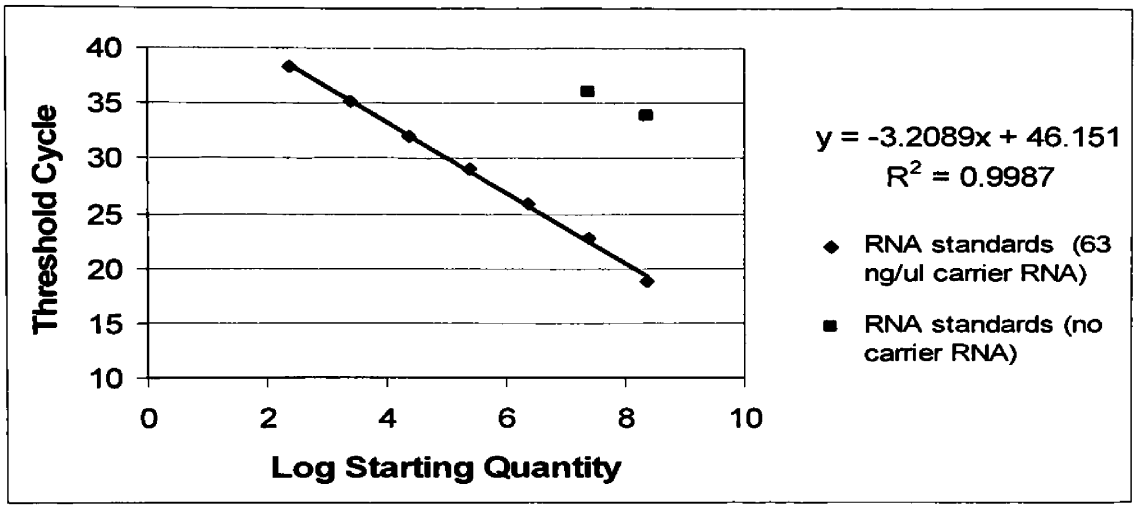

Figure 2.7: Effect of carrier RNA on RT real-time assay. Two RNA standard curves were amplified in parallel, one with carrier RNA and one lacking carrier RNA.

The results indicated that carrier RNA had a greater effect on the amplification efficiencies of the RNA standards than the plasmid DNA standards (Fig. 2.7). The more dilute RNA standards, which did not contain any carrier RNA, did not amplify. These data suggest that either viral RNA was lost during the dilution steps or that the more dilute RNA standards were not efficiently reverse transcribed. For these reasons the addition of carrier RNA was necessary in the RT real-time PCR assay. Carrier RNA alone did not amplify above threshold. Therefore, the viral RNA standards and the viral RNA obtained from the plasma of infected cougars contained the same carrier tRNA concentrations in order to equalize the efficiency of reverse transcription and subsequent amplification.

Comparison of amplification efficiencies

Finally to determine whether the RNA standards and plasma unknowns amplified with equal efficiency, three ten fold dilutions of plasma RNA from a single cougar were amplified in parallel with the RNA standards (Fig. 2.8). The results indicated that the

standards and unknowns amplified with comparable efficiency, 2.02 and 1.88 respectively. The estimated log starting quantities of all three serial dilutions were similar. The range was from 4.5 to 4.85 log starting RNA copies per ml. However, the most dilute plasma unknowns amplified with decreased efficiency. Therefore, the total amount of plasma from each cougar was concentrated through ultracentrifugation prior to amplification to aid in real-time detection.

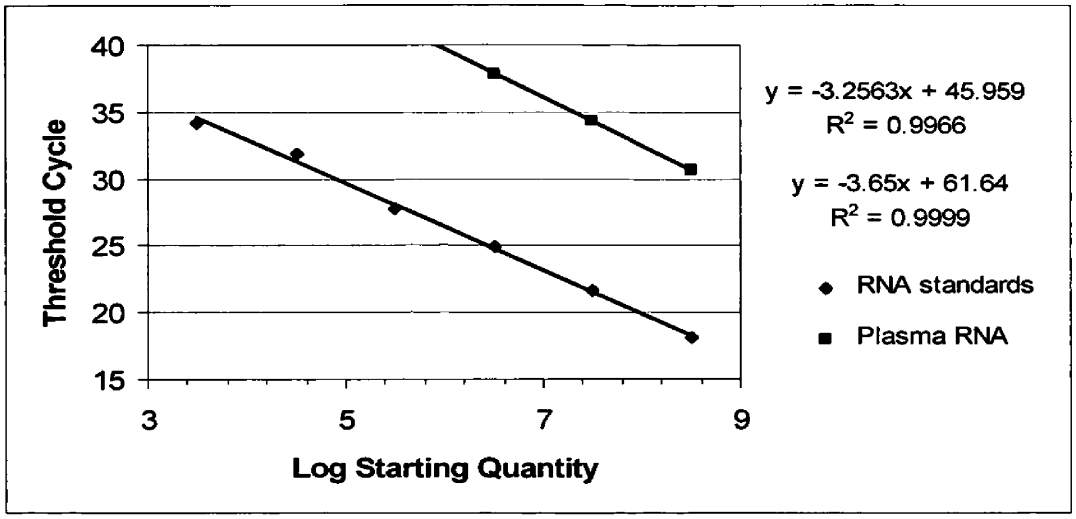

Figure 2.8: Efficiency comparison of RNA standards and plasma unknowns. RNA standards were amplified in parallel with serial ten fold dilutions of plasma from an infected cougars, YM131, to determine whether amplification efficiencies were equal. Efficiency is defined as $10^{-1/slope}$.

The optimized conditions for the real-time FIV_{pco} proviral and plasma viral load assays were subsequently employed to quantify viral loads from a large representative group of infected cougars.

Chapter 3

Manuscript entitled Quantification of Feline Immunodeficiency Virus (FIV_{pco}) in peripheral blood mononuclear cells, lymph nodes and plasma of naturally infected cougars

Introduction

Feline immunodeficiency virus (FIV) is a lentivirus that infects members of the Felidae family worldwide. Although all FIV strains detected in wild and domestic cats form a monophyletic cluster in a phylogeny of lentiviruses, each feline species is infected with a distinct virus and infection results in disparate outcomes (Burkhard & Dean, 2003). FIV is maintained as an apathogenic infection in some members of the cat family such as lions (*Panthera leo*) and cougars (*Puma concolor)* (Brown et al., 1994, Carpenter & O'Brien, 1995, Olmsted et al., 1992). However, FIV infection in domestic cats results in a disease similar to HIV-1 in humans that begins with an acute illness and progresses to immunodeficiency and ultimately death (Bendinelli et al., 1995, Pedersen et al., 1987).

The amount of circulating virus is a strong prognostic indicator for disease progression in FIV and HIV-1 infections (Goto et al., 2002, Mellors et al., 1996). In both naturally and experimentally infected domestic cats, FIV replicates to high titers and elevated viral loads are associated with shorter survival time and progression to feline AIDS (Diehl et al., 1996, Goto et al., 2002). Similarly, high plasma virus loads are associated with disease progression in HIV-1 (Mellors et al., 1996).

African primates are also host to lentivirus infections (simian immunodeficiency virus, SIV) and, as is the case with endemic feline lentivirus infections, there is no

evidence of disease (Beer et al., 1996, Broussard et al., 2001, Chakrabarti et al., 2000). However, plasma virus loads in African green monkeys (*Cercopithecus aethrops*) and sooty mangabeys (*Cercocebus ayts*) naturally infected with SIV_{agm} and SIV_{sm}, respectively, are on the order of 10^6 RNA copies per ml (Broussard et al., 2001, Chakrabarti, 2004). These data indicate that virus replication can be robust even in asymptomatic infections and thus high levels of circulating virus are not always associated with disease.

Currently, no viral load data have been determined for endemic FIV infections in wild felids. FIV_{pco} infects free-ranging cougars in North and South America with infection prevalence averaging 30% (Carpenter et al., 1996), but reaching as high as 58% in some populations in the Western United States (Biek et al., 2003). This prevalence is remarkable because cougars are solitary carnivores with infrequent conspecific contacts. Intrahost viral diversity is less than 1% in infected cougars and the evolutionary rate of FIV_{pco} has been estimated at 0.1-0.3%/site/year (Biek et al., 2003). This is an order of magnitude lower than the estimated rate of 3%/site/year reported for SIV_{agm} (Muller-Trutwin et al., 1996) or 1%/site/year for HIV-1 (Leitner & Albert, 1999, Poss et al., 2004, Shankarappa et al., 1999). The faster evolutionary rate of SIV and HIV-1 could be due to increased viral replication resulting in a rapid accumulation of mutations and stronger selection on the virus population. Therefore, based on the lack of disease, the low intrahost viral diversity and low evolutionary rates, we hypothesized that viral loads in cougars would be lower than in pathogenic FIV and HIV-1 infections or in endemic SIV infection in primates. We subsequently developed a real-time PCR assay for FIV_{pco} and

used the assay to determine the amount of virus present in a large set of naturally infected cougars.

Methods

Study Population and Cougar Samples

Peripheral blood mononuclear cells (PBMC), lymph nodes (LN) and plasma samples used in this study were obtained from free-ranging cougars from four Rocky Mountain populations previously determined to be infected with FIV_{pco}. Genomic DNA samples from PBMC were obtained from 39 infected cougars. Genomic DNA samples from LN were obtained from a group of 10 hunter-killed animals submitted to the Montana Department of Fish, Wildlife, and Parks. Plasma samples were also obtained from 32 infected cougars. Genomic DNA was extracted from samples as previously described (Biek et al., 2003).

Phylogenetic analysis

A fragment of proviral *env* was amplified from serial dilutions of PBMC or lymph node DNA from all infected cougars evaluated in this study. PCR products were cloned and sequenced as previously described (Biek et al., 2003). Alignments were conducted in Lasergene (version 5.5) from DNASTAR, Inc (Madison, WI) using the CLUSTAL W algorithm. A maximum likelihood (ML) tree was created in PAUP* (4.10b; Sinauer Associates, Inc.) (Swofford, 2002) using a GTR+I+G model as determined in Modeltest (Posada & Crandall, 1998). PLV1695 (AY307116) was used as an outgroup (Biek et al., 2003). 100 bootstrap iterations were performed. One *env* sequence for each cougar has

been submitted to Genbank under accession numbers AY120787, AY120790, AY120793-94, AY120798-802, AY120804-810, AY120812, AY120815, DQ106994-97, DQ106999-00, DQ107003-06, DQ107052-54, DQ107056-60 and DQ107062-68.

Sequence analysis of the real-time FIV_{pco} amplicon

A 690 bp fragment of proviral FIV_{pco} was amplified by nested PCR from DNA derived from PBMC of 14 infected cougars, which included representatives of each viral lineage. The oligonucleotides used for the first round were Co7990F (5'-ATGCAAGTTATGAGATGTAG-3' and Co8958R (5'-TTATTCAACCGTTCGCACTT-3'). The oligonucleotides used for the second round were Co3LTRF (5'-ACGGCCTTAGTGGTGTCTCAG-3') and Co8859R (5'-CCATTCCTCCCAGTCTACCC-3'). The conditions for the first round of PCR were as follows: 3 min at 94°C followed by 35 cycles of 94°C for 30 sec, 48°C for 30 sec, 71°C for 70 sec and followed by a 5 min extension at 71°C. The conditions for the second round of PCR were as follows: 3 min at 94°C followed by 35 cycles of 94°C for 30 sec, 51°C for 30 sec, 71°C for 45 sec and followed by a 5 min extension at 71°C. The PCR products were cloned into the pDrive plasmid (Qiagen, Velencia, CA) and sequenced.

Plasma Viral RNA Preparation

Plasma or serum samples were centrifuged for 1.5 h at 100,000 x g. The viral pellet was resuspended in 140 µl PBS containing Ca^{+2} and Mg^{+2} and incubated for 1 h with DNase. RNA was purified using the QIAamp viral RNA mini kit (Qiagen) and

eluted in 30 µl DEPC-treated water. Plasma volumes greater than 2 ml were eluted in 60 µl. Samples were stored at -80°C for cDNA synthesis.

Preparation of DNA and RNA real-time PCR Standards

A plasmid standard for myosin was constructed by amplifying a 220 bp fragment of cougar genomic DNA with primers designed to exon 19 of the cougar myosin gene. The primers used were MyoF (5'-CAAGAACTGGCCCTGGATGAA-3') and MyoR (5'-CTGCACTTGGAGCTGGAGGTC-3'). The conditions for the PCR were as follows: 3 min at 94°C followed by 30 cycles of 94°C for 30 sec, 52°C for 30 sec, 71°C for 50 sec and followed by a 5 min extension at 71°C. The PCR product was cloned into the pCR4-Topo plasmid (Invitrogen, Carlsbad, CA). A 690 bp fragment of the FIV_{pco} genome near the 3' end of *env* was amplified by PCR from cougar proviral DNA as described above. All plasmids were linearized and purified with the QIAquick PCR Purification Kit (Qiagen). Plasmid concentration was determined by UV spectroscopy. All DNA plasmid standards were diluted in 10 mM Tris containing salmon sperm DNA (Sigma-Aldrich, St. Louis, MO) as a carrier at a final concentration of 6 ng/µl.

Virus from the supernatant of a coculture of 3201 cells and PBMC of a naturally infected cougar, SRF631, was used for the RNA standards. Viral RNA concentration was determined by UV spectroscopy to estimate copy number. All RNA standards were diluted in DEPC-treated water and carrier tRNA (Sigma) at a final concentration of 63 ng/µl. The viral RNA standards and viral RNA obtained from the plasma of infected cougars contained equivalent carrier tRNA concentrations.

FIV_{pco} Real-time PCR Quantification

TaqMan chemistry was used to quantify the number of cell equivalents in each proviral reaction. For the myosin reactions, the primers used were MyoTaqMF (5'-TGGCCCTGGATGAAACTCTACT-3') and MyoTaqMR (5'-GCCATCTCCTTCTCGGTCTCT-3'). The probe sequence used for this primer set was Myoprobe (5'-FAM-CAAGATCAAGCCCCTCCTCAAGAGCG-TAMRA-3').

SYBR green chemistry was used for quantification of FIV_{pco} from genomic DNA and plasma because sequence divergence among FIV_{pco} lineages precluded designing a suitable probe. The primers used were ETaqF (5'-TGATCCTGATGCTCCACCAAC-3') and ETaqR (5'-TCTCACTCTGTTCTGCCCATT-3'). The amplification with this pair of oligonucleotides produced a fragment of 170 bp.

Reactions consisted of 25 µl of the 2X Universal Master Mix (Applied Biosystems, Foster City, CA) containing 100 mM KCl, 40 mM HCl Tris, 1.6mM dNTP, 50 Units/µl Taq, 6 mM $MgCl_2$ and 5 µl of genomic template, in a 50 µl total reaction volume. Each myosin reaction contained 300 nM MyoTaqMF, 100 nM MyoTaqMR and 50 nM Myoprobe. Each FIV_{pco} proviral reaction contained 300 nM ETaqF, 300 nM ETaqR and 1:10000 dilution of SYBR Green I gel stain (BioWhitaker, Walkersville, MD).

Myosin amplification was 1 cycle of 95°C for 10 min followed by a two-step PCR procedure consisting of 95°C for 15 sec then 60°C for 1 min for 45 cycles. FIV_{pco} amplification was similar except that the annealing temperature was 61°C for 1 min. Amplification, data acquisition and analysis were performed using the iCycler real-time PCR detection system (BioRad, Hercules, CA). All FIV_{pco} reactions were evaluated by

melt curve analysis to confirm the size of the amplicon and lack of primer dimer formation. Genomic DNA from uninfected cougars did not amplify with FIV_{pco} specific oligonucleotides.

Reverse transcription (RT)-PCR was carried out as a two-step procedure for both the RNA standards and plasma samples. The reaction mixture, 30 µl total, contain 1 µl SuperScript™ III Reverse Transcriptase (Invitrogen), 4 µl 5X RT buffer, 1 nM ETaqR and 10 µl purified RNA. The reaction was conducted at 50°C for 50 min. and 85°C for 5 min.

Plasma viral RNA quantification was determined using 50 µl reactions consisting of 25 µl 2X Platinum SYBR Green qPCR SuperMix (Invitrogen), 300 nM ETaqF and 300 nM ETaqR. FIV_{pco} amplification was 1 cycle of 50°C for 2 min followed by 1 cycle of 95°C for 2 min then a two-step PCR procedure consisting of 95°C for 15 sec then 60°C for 45 sec for 45 cycles.

All standards, negative controls and samples were run in duplicate and the average value of the copy number was used to quantify both FIV_{pco} and myosin. The measurements of myosin and FIV_{pco} copy numbers were accepted if the coefficients of variation (CV) were <20% for myosin reactions and <35% for FIV_{pco} reactions. FIV_{pco} copy number for provirus was divided by the number of cells assayed and reported on the basis of 10^6 PBMC or LN cells. FIV_{pco} copy number for plasma virus was divided by the volume of plasma assayed and reported as the number of viral RNA copies per milliliter of plasma.

Statistical Analysis

The lower limits of detection for the proviral and plasma viral load real-time PCR assays were set at 100 DNA copies and 320 RNA copies per reaction to account for increased variability in cycle number in quantifying low copy numbers (see Results). Samples that amplified below the lower limit of detection were confirmed by melt curve analysis.

Proviral and plasma viral loads were determined from PBMC and plasma that were above the lower limit of detection. The mean and standard deviation of both proviral and plasma viral loads were calculated. 95% confidence intervals were then set for both population means through the Student's *t* distribution. The lower limit of both proviral and plasma viral loads was calculated. The minimum number of cell equivalents and minimum volume of plasma per reaction, which would generate viral loads within the 95% confidence intervals, were determined to be 1.16×10^4 cells and 100 µl plasma per reaction. Samples assayed that exceeded the calculated minimum of cell equivalents or plasma volume, but had viral loads below the lower limit of real-time detection, were down weighted with a factor of $1/\sqrt{10}$ to account for increased variability in threshold cycle numbers at low copy number. Proviral and plasma samples assayed below the calculated minimum of cell equivalents or plasma volume and samples that did not reach threshold were excluded from the statistical analysis.

A weighted univariate analysis of covariance (ANCOVA) was used to test if any significant differences existed among the $\log_{10}$ proviral and plasma viral load means due to differences in age, gender and lineage. Levene's test of equality of error variance was used to ensure equal variance existed across the lineages. The proviral model was created

based on the ANCOVA of proviral load on age, which resulted in separate slopes and intercepts for each lineage.

Results

Experimental conditions of the FIV_{pco} proviral and plasma viral load real-time PCR assays

A fragment of exon 19 of the cougar myosin gene was used to determine the number of cell equivalents in samples to be quantified for FIV_{pco} provirus. Amplification of the myosin standard curve was based on Taqman chemistry and was linear over seven orders of magnitude. To determine if amplification of the plasmid standards and genomic DNA was equivalent, the myosin standard curve was compared to a 10-fold dilution series of cougar genomic DNA that spanned the range of genomic DNA concentrations used to estimate the number of cell equivalents (data not shown). The efficiencies (defined as $10^{-1/slope}$) of the plasmid and genomic samples were 1.90 and 1.91 respectively, indicating that plasmid and genomic DNA amplified with equivalent efficiency in our assay. The number of cell equivalents determined for proviral quantifications was established by calculating the mean of two separate myosin quantifications of genomic cougar DNA.

The inter-assay variation for myosin quantification was determined by comparing the values obtained for standard curves amplified in four separate experiments. Five standards with the lowest copy number ($9.25x10^4$ to $9.25x10^0$ copies per reactions) were used in calculating the CV to measure the variation in the most dilute standards (data not

shown). The average threshold cycle (Ct) CV was 1.04% and the average absolute CV was 14.52%. These results demonstrate that the assay used to enumerate cell equivalents is highly reproducible.

Previous work established that mismatches within the real-time primer sites do not enable accurate quantification because of variable efficiencies in amplification (Klein et al., 1999, Leutenegger et al., 1999). Therefore, since the viral sequence diversity observed among cougar lentiviurses is greater than the diversity observed in FIV in domestic cats (Carpenter et al., 1996), we considered it necessary to first establish the phylogenetic affiliation of all FIV_{pco} samples prior to quantification and then determine the effect of nucleotide mismatches on FIV_{pco} real-time amplification. All samples clustered within five distinct viral lineages based on a fragment of *env* (Fig. 3.1). Viral lineage associations were consistent with those in a ML tree of 150 individual cougar sequences from data sets based on *env* and *pol* (unpublished data). The associations of lineage one and two were consistent with previously published results (Biek et al., 2003, Carpenter et al., 1996). The sequence variation in the FIV_{pco} amplicon primer sites was then determined from a representative subset of infected cougars from each viral lineage (Fig. 3.2). The viral sequence from lineage four was an exact match to the primers. The sequences from lineage one and three had the same single mismatch in the reverse primer. The standard from lineage two had a single mismatch in the forward primer and the standard from lineage five had single mismatches in both the forward and reverse primer sites.

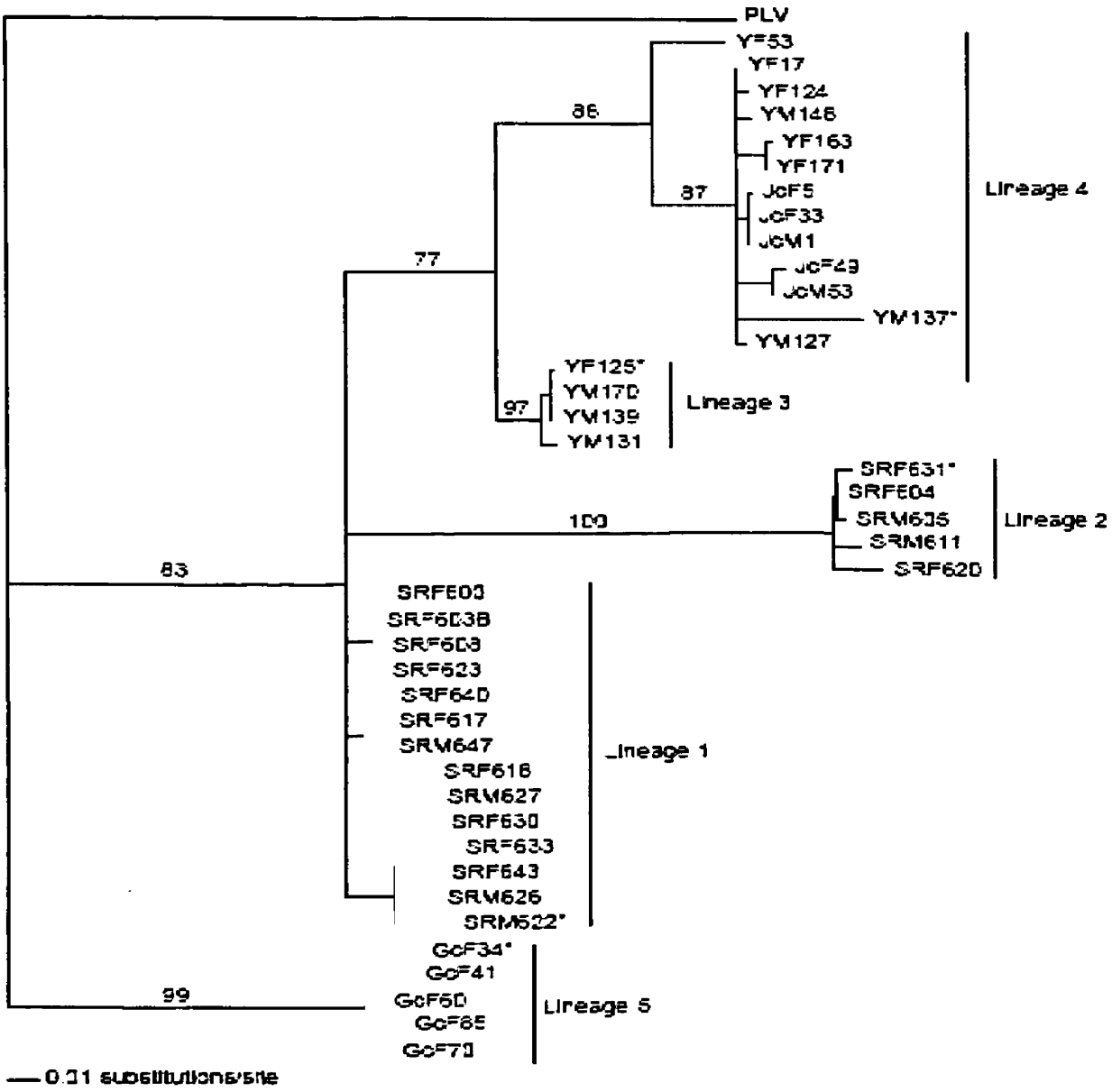

Figure 3.1: Phylogenetic relatedness of FIV_{pco} based on *env*. An estimate of the phylogenetic relationship of partial FIV_{pco} *env* sequences from naturally infected cougars based on maximum likelihood. The values next to the tree nodes represent bootstrap values of ≥ 70 based on 100 bootstrap iterations. PLV was used as an outgroup. The population affiliation and sex for each cougar is indicated before the animal identification

number (Y, Yellowstone National Park, MT; SR, Snowy Mountain Range, WY; Gc, Garnet Mountain Range, MT; Jc, Jackson Mountain Range, WY). Sequences used in real-time proviral quantification as plasmid DNA standards are indicated by *.

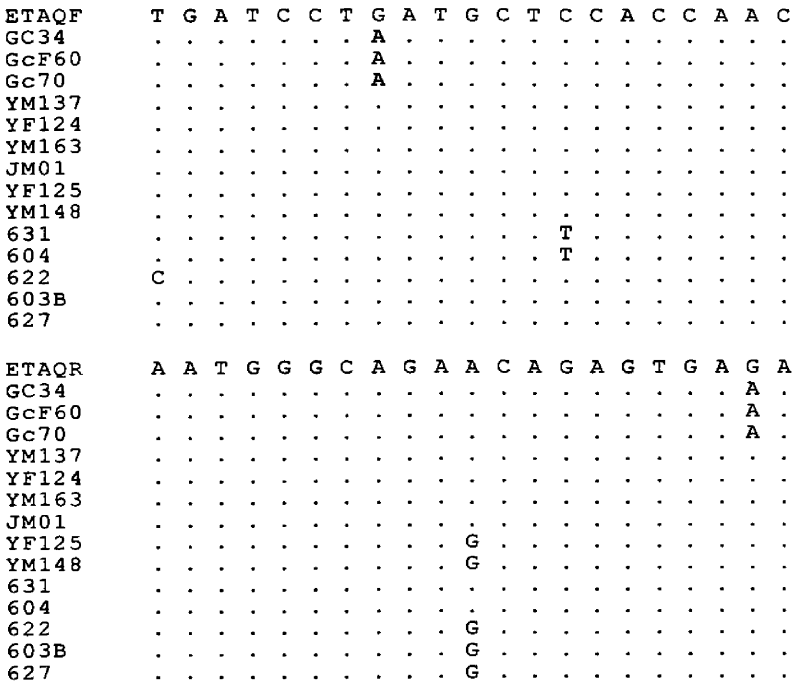

Figure 3.2: Sequence variation of FIV_{pco} in the forward and reverse primer sites. The alignment shows the number of nucleotide mismatches within the primer sites from a representative subset of naturally infected cougars for each viral lineage. Both primer sequences are shown in the sense orientation. Dots indicate match with the primer sequences.

We prepared separate FIV_{pco} standards from sequences that represented each viral lineage and investigated the effects of these mismatches on amplification efficiency. Lineage standards containing no mismatches, or mismatches in one or both primers were evaluated simultaneously by real-time PCR. Standards from three lineages produced overlapping curves (Fig. 3.3a) and were not significantly different based on a *F* test for significant differences between lines ($P = 0.114$). Although the differences between DNA

plasmid standard curves were not significantly different, the error associated with the low copy number standards increased with the number of primer mismatches. Therefore, for proviral DNA quantification, a lineage specific standard was used for samples of each lineage.

The average Ct CV (3.62%) and the average absolute CV (38.52%) was calculated to determine FIV_{pco} inter-assay variation (Fig. 3.3b). The inter-assay variation of the FIV_{pco} real-time assay was greater than the difference between different FIV_{pco} lineage standards. The average absolute FIV_{pco} inter-assay variation, obtained with SYBR green, of 38.52% is comparable to the variation previously described in real-time assays using Taqman probes, which has been reported to be greater than 35% (Damond et al., 2001, Desire et al., 2001). As seen in Figure 3.3b, the coefficient of variation increased at the lowest copy numbers, where the final standard, $6.45x10^1$ copies, had the largest CV value (68.33%). Subsequently, we set the lower limit of detection at 100 DNA copies per reaction to account for the variability associated with the most dilute standard.

A

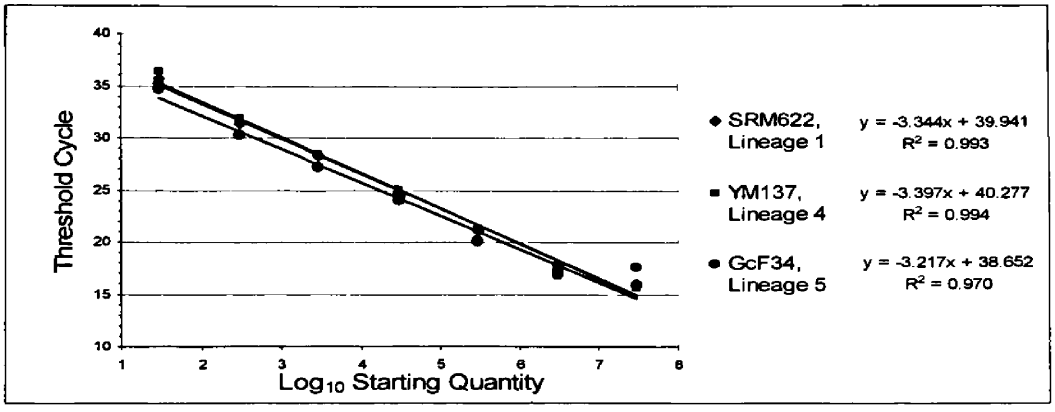

Standard	Efficiency	Mismatches	Copy Number at Ct = 30	Percent Decrease from YM137

GcF34	2.04	1 for / 1 rev	489	53.8%
SRM622	1.99	1 rev	939	11.4%
YM137	1.96	None	1060	N/A

B

Copy Number per reaction	Ct mean	SD	%CV	Abs mean	SD	%CV
$6.45X10^5$	20.04	0.95	4.72	798220	210341	26.35
$6.45X10^4$	23.27	0.72	3.08	78042	22146	28.38
$6.45X10^3$	26.59	0.86	3.22	7468	2979	39.89
$6.45X10^2$	30.24	0.83	2.74	515	153	29.71
$6.45X10^1$	33.21	1.45	4.36	60	41	68.33

Figure 3.3: Real-time FIV_{pco} proviral standard curves and inter-assay variation. A) A comparison of FIV_{pco} DNA standard curves amplified from plasmid standards representing three viral lineages. The amplification efficiency and the number of primer mismatches are indicated for each standard. Copy number at Ct = 30 denotes the number of proviral copies calculated from each plasmid standard curve at threshold cycle 30. B) The inter-assay variation in the SYBR green proviral quantification assay was determined for the most dilute standards in order to establish the effect of low copy number on inter-assay variation. Ct mean = mean value for threshold cycle number, SD = standard deviation, %CV = coefficient of variation expressed as a percentage, Abs mean = mean value for absolute copy number.

For plasma viral load quantification, a two-step real-time PCR assay was developed that was linear over six orders of magnitude from $3.2x10^8$ to $3.2x10^2$ copies (Fig. 3.4). The lower limit of detection for this assay was set at 320 RNA copies per reaction to account for increased variation in threshold cycle number with low copy

number standards. Only one RNA standard was amplified in the real-time reverse transcription (RT) assay because there were no significant differences between separate proviral standards in amplification and virus representative of all five lineages have not been isolated. Because we did not know *a priori* if we would detect any circulating virus in cougar blood, the total amount of plasma was concentrated by ultracentrifugation before RNA isolation to aid in detection. Standards and samples were reverse transcribed simultaneously to ensure similar RT efficiencies within an assay. The inter-assay variation for RT real-time PCR was 3.92% for the average Ct CV and 38.38% for the average absolute CV (Fig. 3.4). This is similar to the inter-assay variation for the proviral quantification suggesting that the RT step had minimal effects on assay reproducibility and is also comparable to variation reported for other real-time RT assays (Gibellini et al., 2004, Gueye et al., 2004).

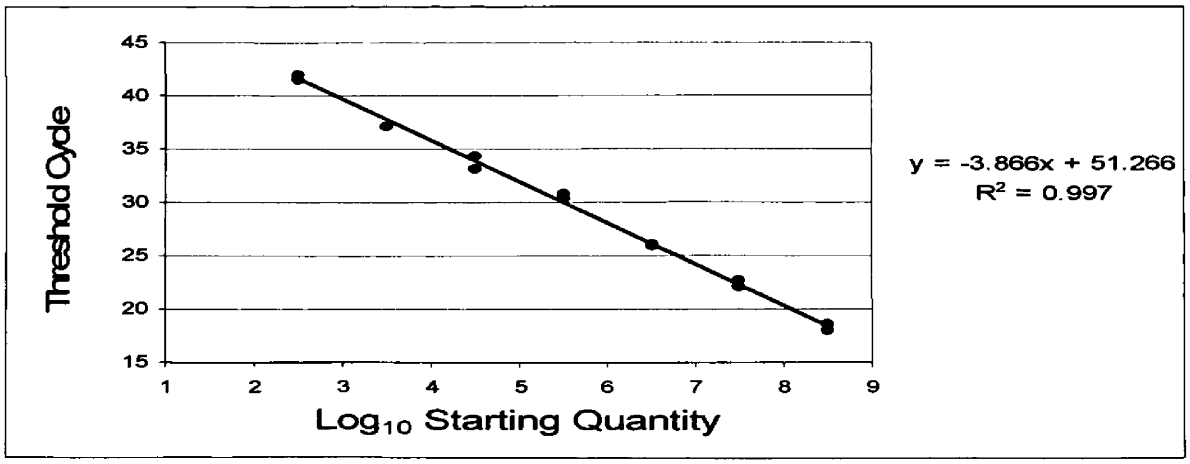

Copy Number per reaction	Ct mean	SD	%CV	Abs mean	SD	%CV
$3.2X10^6$	25.44	0.76	2.99	4050897	1446616	35.71
$3.2X10^5$	29.51	1.18	3.99	231206	61939	26.79
$3.2X10^4$	32.40	1.12	3.45	30121	9216	30.60
$3.2X10^3$	34.49	1.49	4.31	6825	3484	51.05
$3.2X10^2$	40.50	1.96	4.85	199	95	47.74

Figure 3.4: Real-time FIV_{pco} RNA standard curve and inter-assay variation. The RNA standard curve shown is from a representative two-step SYBR green RT-PCR real-time experiment. The inter-assay variation of the two-step SYBR green RT real-time assay was determined for the most dilute standards in order to establish the effect of low copy number on inter-assay variation. FIV_{pco} genomic RNA was prepared from the supernatant of a coculture of PBMC from SRF631, a cougar infected with a lineage 1 virus, and a domestic cat cell line.

Proviral Loads in naturally infected cougars

Cougar samples quantified in this study were previously determined to be FIV_{pco} positive by nested PCR. Therefore, the FIV_{pco} real-time PCR assay was utilized only to quantify viral loads and was not used as a detection method. Thirty-nine cougar PBMC samples were quantified and 22 (56%) were within our level of detection. Ten lymph node (LN) samples were also quantified and five were within the range of detection (50%). Samples that had less than 100 proviral copies, which we established as the lower limit of detection, were still valuable in our analysis. For example, FIV_{pco} copy number was below the limit of detection in four PBMC and two LN samples despite the fact that more than $1x10^5$ cell equivalents were assayed, indicating that the proviral load was low in those animals. Therefore, 95% confidence intervals for the number of cells required for FIV_{pco} detection was established (see Materials and Methods). Samples that were adequately assayed but below detection were down weighted to account for increased

variability associated with threshold cycle number. Eight PBMC samples were down weighted in the proviral analysis. Samples for which there were insufficient cell numbers or plasma volume for adequate sampling were omitted from the statistical analysis. Nine PBMC samples were omitted from the proviral analysis.

The mean proviral load per 10^6 PBMC was $1.34x10^4$ and ranged from $2.9x10^1$ to $6.72x10^4$ (Fig. 3.5). The lowest proviral loads were adequately assayed, however, the number of proviral copies quantified was below our limit of detection. Therefore, these samples were down weighted. The mean proviral load per 10^6 lymph nodes cells was $1.51x10^4$ (range $8.06x10^3$ to $2.51x10^4$). These data indicate that an average of 1 in 75 circulating cells is infected with FIV_{pco} and 1 in 66 cells in the lymph nodes are infected.

We tested the hypothesis that average proviral loads in PBMC were equal among gender, age and lineage using a weighted ANCOVA. These factors were considered because one or all may have a significant biological effect on the amount of virus in infected cougars. Previous experimental FIV infections established that the amount of virus in domestic cats differs significantly between different field isolates (Pedersen et al., 2001). Therefore, it was important to understand whether these factors influence viral loads in natural endemic FIV infections. The variation in proviral load was determined to be equal across lineages through Levene's test of equality of error variance ($P = 0.239$). Proviral loads were significantly different between lineages ($P = 0.029$) and there was a significant interaction between viral lineage and cougar age, indicating that these variables considered together had an effect on proviral load ($P = 0.014$). No correlation was observed between proviral load and gender ($P = 0.440$).

Univariate analysis of covariance demonstrates whether differences between means are statistically significant but not how means differ. Therefore, to understand the influence of age and lineage on proviral loads, the linear regression from the ANCOVA of proviral load on age was conducted to model the change in lineage specific proviral loads versus age, which resulted in separate curves for each lineage ($R^2 = 0.549$) (Fig. 3.6). Cougars infected with viruses from either lineage one or two have an increase in PBMC proviral loads with age. In contrast, cougars infected with viruses from either lineage three, four or five exhibit a decrease in proviral loads with age. The linear regression of proviral loads from lineages one and two were statistically different from those of lineages three, four and five ($P \leq 0.05$). However, the differences observed between lineages three, four and five were not significant ($P > 0.24$).

Plasma Viral Load in naturally infected cougars

Thirty-two plasma samples were quantified and in 21 (66%) of these samples FIV_{pco} was detectable in our real-time assay. The plasma viral loads ranged from $2.30x10^3$ to $2.81x10^6$ RNA copies per ml, with a mean of $5.69x10^5$ (Fig. 3.5). Of the 11 plasma samples that were below our limit of detection, eight samples were not included in the statistical analysis because an insufficient volume of plasma was assayed and three samples were down weighted as previously described. The variance in plasma viral loads was determined to be equal across lineages through Levene's test ($P = 0.086$). Moreover, through a univariate ANCOVA, no significant differences were observed between mean plasma viral loads for different genders, ages or lineages ($P = 0.958$, 0.830 and 0.783 respectively). Additionally, we were able to quantify proviral and plasma viral loads from

the same blood sample of 11 cougars in the study (Fig. 3.7). As is evident from Figure 6, no correlation was observed between proviral and plasma viral loads (R^2 value = 0.133). These data demonstrate that FIV_{pco} infected cells produce variable amounts of virus in the blood, which is not correlated to the number of infected PBMC, age, gender or viral lineage.

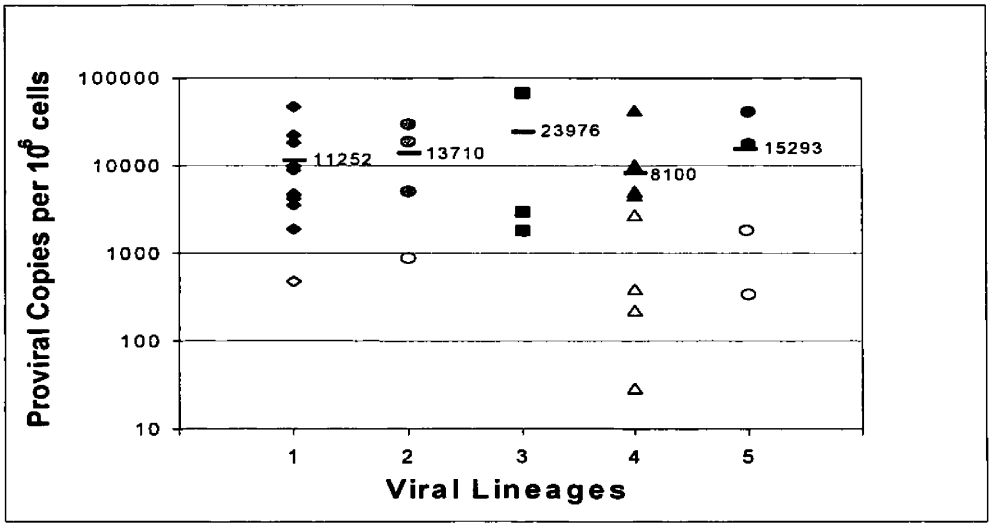

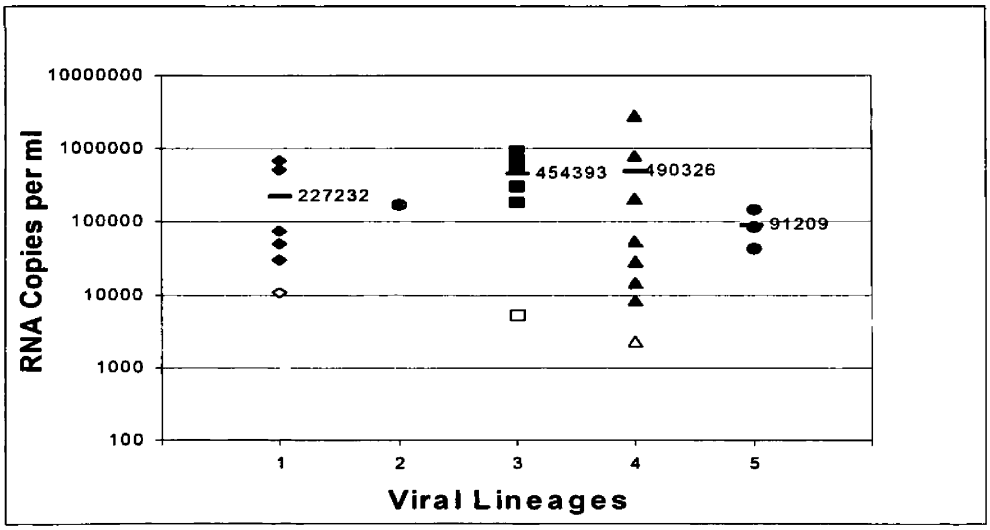

Figure 3.5: FIV_{pco} proviral and plasma viral load for each viral lineage. The average values for each viral lineage are shown next to the horizontal lines. Closed shapes denote proviral or plasma viral loads that were within the detection limits established for this assay. Open shapes denote down weighted proviral or plasma viral loads.

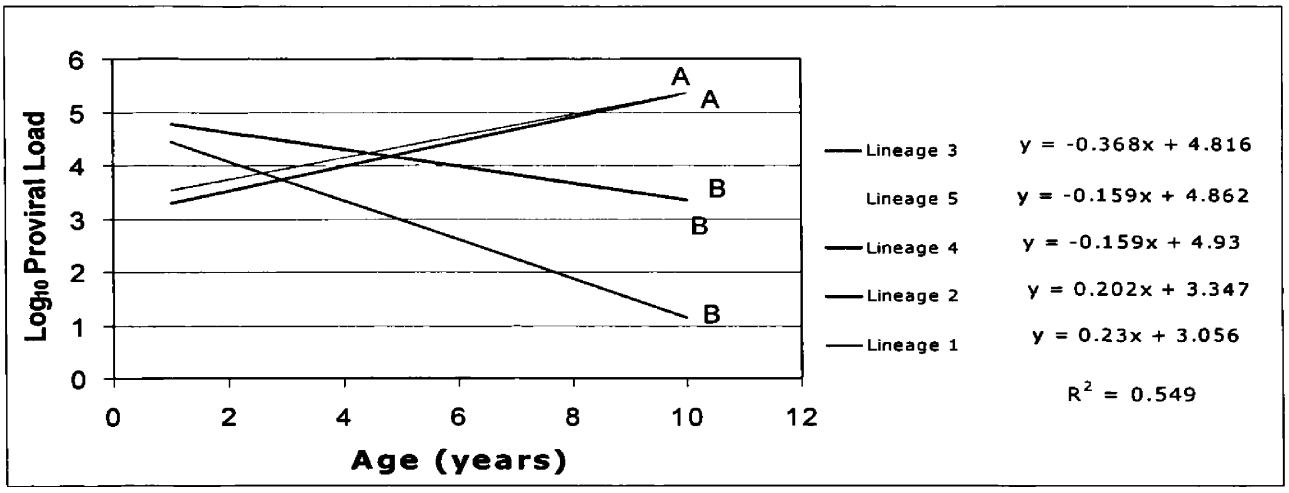

Figure 3.6: A weighted analysis of covariance of cougar PBMC proviral loads versus cougar age. The colors for each viral lineage correspond to the phylogeny displayed in Fig. 1. The change in lineage specific proviral loads versus cougar age was based on an ANCOVA of cougar PBMC proviral loads with viral lineage and gender as factors and age as a covariate. Lineage specific PBMC proviral loads were averaged across gender because gender was not a significant influence on PBMC proviral loads. The linear regressions of proviral loads from lineages one and two, indicated with A, were statistically different from those of lineages three, four and five ($P \leq 0.05$). However, the differences observed between lineages three, four and five, indicated with B, were not significant ($P > 0.24$).

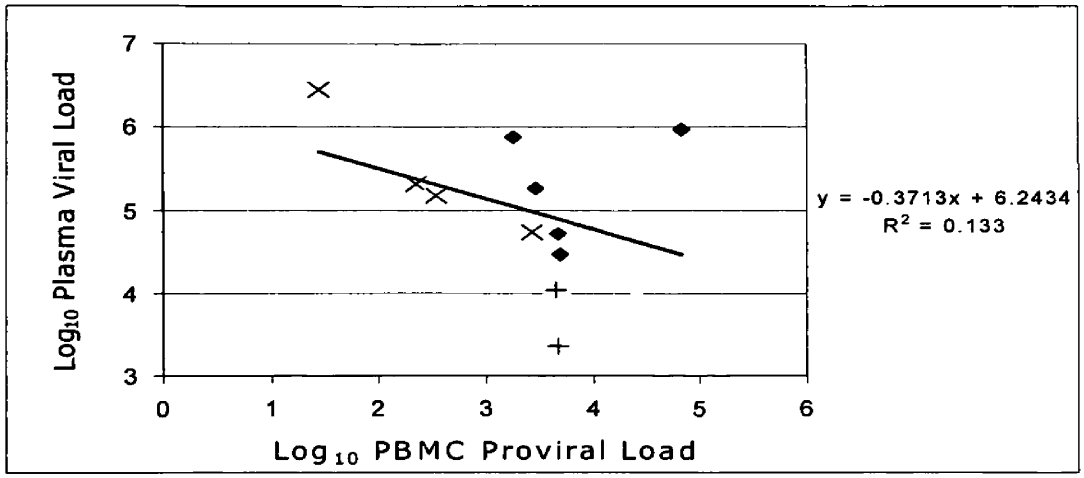

Figure 3.7: Correlation of cougar PBMC proviral loads versus plasma viral loads of infected cougars. Proviral and plasma viral loads were quantified from the same blood

sample of 11 cougars. All samples had at least one viral load parameter that was within the detection threshold. Diamonds denote proviral and plasma viral loads within the detection threshold. Down weighted proviral loads are indicated with 'x' and '+' denotes down weighted plasma viral loads.

Discussion

Free-ranging cougars are one of many feline species that harbor an endemic lentivirus infection without any apparent signs of disease (Carpenter & O'Brien, 1995, Olmsted et al., 1992, Troyer et al., 2004). However, it was not known if the lack of disease observed in naturally infected cougars was a result of low level viral replication. Consequently, FIV_{pco} proviral and plasma viral loads were quantified from naturally infected cougars through a recently developed real-time PCR assay. This study represents the most extensive analysis of proviral and plasma viral loads in natural, endemic lentivirus infections to date.

Proviral loads previously reported in infected PBMC from African green monkeys and sooty mangabeys are on the order of 10^2 to 10^3 proviral copies per 10^6 cells, respectively (Beer et al., 1996, Broussard et al., 2001, Chakrabarti, 2004, Muller & Barre-Sinoussi, 2003, Rey-Cuille et al., 1998). The average cougar PBMC proviral load was 1.34×10^4 proviral copies per 10^6 cells. Therefore, FIV_{pco} proviral loads in infected PBMC are an order of magnitude higher than in PBMC from infected primates. The average LN proviral load, which was determined from a separate group of infected cougars, was 1.51×10^4 proviral copies per 10^6 cells. Although the variation around LN proviral loads was markedly lower than in PBMC, both cougar PBMC and LN cells had similar average proviral loads. Equivalent PBMC and LN proviral loads have been previously reported in a large cohort of long-term naturally infected AGM (Beer et al.,

1996). These data stand in contrast to other studies that have reported elevated proviral loads in lymphoid tissue in naturally infected primates and HIV-1 infected humans (Broussard et al., 2001, Fauci et al., 1996, Rey-Cuille et al., 1998). Finally, plasma viral loads in naturally infected cougars ranged from 10^3 to 10^6 RNA copies per ml and are comparable to viremia levels previously reported in SIV_{sm} and SIV_{agm} infections (Broussard et al., 2001, Goldstein et al., 2000, Holzammer et al., 2001, Rey-Cuille et al., 1998). These data clearly indicate that the absence of detectable disease in naturally infected cougars and primates is not a result of low level viral replication.

In epidemic lentivirus infections, such as HIV-1 or FIV in domestic cats, the amount of circulating virus is an accurate predictor of disease severity. In humans and domestic cats, plasma viral loads greater than 10^5 copies per ml are correlated to disease progression and shorter survival time (Diehl et al., 1996, Goto et al., 2002, Mellors et al., 1996). FIV_{pco} infected cougars maintain plasma viral loads that are greater than 10^5 copies per ml during infection, but these animals remain asymptomatic. Since elevated plasma viral loads in infected cougars are not associated with disease, we determined whether FIV_{pco} plasma viral loads were influenced by factors such as age, gender or viral lineage. However, no significant differences were observed. The lack of correlation in plasma viral loads to these factors may reflect the transient nature of cell-free virus compared to the integrated provirus. Different rates of cell-free virus clearance and production have been reported in patients infected with HIV-1, but the lifespan of infected cells were not significantly different among patients (Perelson et al., 1996). Therefore, if the amount of virus in the blood varies between infected animals, detecting

a correlation between plasma viral loads and certain factors in a wild population would be difficult.

FIV_{pco} plasma viral loads were also evaluated in comparison to PBMC proviral loads from 11 infected cougars to determine whether a correlation existed between these two viral compartments though no correlation was observed. In fact the animal with the highest plasma viral load ($2.81x10^6$) maintained a proviral load that was below the lower limit of detection (Fig. 7). These data suggest that FIV_{pco} may not be produced from circulating PBMC. This is consistent with HIV-1 infections where the primary site of virus production is lymphoid tissue (Haase, 1999) and greater than 90% of HIV-1 plasma viremia is maintained by a fraction of the $CD4^+$ T cell population (Ho, 1997, Hufert et al., 1997).

The large sequence divergence and widespread distribution of FIV_{pco} in North America indicate that FIV_{pco} has co-evolved with its cougar host for a long time (Carpenter et al., 1996). The high cell-associated and cell free viral loads documented in infected cougars may be an effective mechanism by which FIV_{pco} can sustain a high prevalence rate (30-58%) in a solitary species (Carpenter et al., 1996). Indeed, both FIV cell-associated and cell free virus are able to cause infection in domestic cats (Burkhard & Dean, 2003, Burkhard et al., 1997). Furthermore, previous FIV_{pco} studies established that negative selection, which constrains genetic diversity, dominates in FIV_{pco} infections (Biek et al., 2003). Thus the low intrahost viral diversity reported appears to be the result of an absence of strong positive selection on the virus and not to low levels of viral replication.

Our results indicate that a large proportion of the variability in PBMC proviral loads can be ascribed to viral lineage and cougar age ($R^2 = 0.549$). Although the number of PBMC samples quantified was moderate (n = 30), there was a strong correlation between PBMC proviral loads to viral lineage and cougar age ($P = 0.014$). Because differences in proviral loads among viral lineages were most pronounced in adult cougars (Fig. 6), changes in hormone levels associated with sexual maturation or activity may influence viral replication. Activation of viral transcription occurs in type B (mouse mammary tumor virus) and type C (murine leukemia virus) retroviruses in response to adrenal steroids by binding their respective receptors to hormone response elements located within the long terminal repeat (LTR) (Cato et al., 1988, Miksicek et al., 1986). Therefore, the physiological state of a maturing infected cougar may influence viral replication and ultimately affect the number of infected circulating cells. Such a replication strategy could optimize viral transmission during contact events. Interestingly, animals infected with viruses from lineage one and two, which displayed an increase in proviral load with age, are from the population with the highest prevalence of FIV_{pco} infection (Biek et al., 2003), suggesting that this strategy leads to a higher likelihood of transmission.

In summary, quantification of FIV_{pco} proviral and plasma viral loads has established that infected cougars maintain substantial viral loads that are comparable or higher than those reported in endemic primate lentivirus infections. These data further support the premise that high levels of lentiviral replication do not necessarily correlate with disease. Finally, differences observed in cougar PBMC proviral loads correlated to

viral lineage and host age suggesting that different life strategies exist within FIV_{pco} lineages.

Chapter 4:

Conclusions and Future Prospects

The quantification of FIV_{pco} proviral and plasma viral loads provided necessary information about the amount of virus maintained in an endemic lentivirus infection in cougars. The study also represented the largest viral load study from a naturally infected wild population. Interestingly, significant differences observed among cougar PBMC proviral loads correlated to viral lineage and cougar age. Because differences in proviral loads among viral lineages were most pronounced in adult cougars, we hypothesize that sexual maturation may influence viral replication (see Chapter 3, Discussion). In animals sexual maturation is associated with an increase in hormone levels, which may differentially influence FIV_{pco} viral replication and result in distinct PBMC proviral loads among infecting viral isolates.

Adrenal steroids have been previously shown to both increase and decrease viral replication in distinct lentivirus infections. For example, adrenal steroids have been previously shown to induce the transcription of type B (mouse mammary tumor virus, MMTV) and type C (murine leukemia virus, MLV) retroviruses (Cato et al., 1988, Miksicek et al., 1986). In contrast, glucocorticoid dexamethasone (DXM), a steroid hormone that binds the glucocorticoid receptor, blocks the activation of HIV-1 replication in chronically infected cell lines and infected PBMC (Laurence et al., 1989, Mitra et al., 1993). Steroid hormones exert their effect on viral transcription by binding their respective receptors, translocating to the nucleus and binding hormone response elements located within the long terminal repeat (LTR) of the proviral DNA.

In addition to the significant differences observed among PBMC proviral loads, FIV_{pco} lineages differ genetically within their LTR response elements (data not shown). Consequently, the possibility exists that separate FIV_{pco} isolates may respond differentially to hormone treatment. Therefore, future experiments may entail *in vitro* studies to investigate the effect of hormones on viral transcription and replication.

For example, cultured cougar cells infected with separate viral isolates could be stimulated with a series of steroid hormones to determine whether infected cells respond differentially to hormone treatment. Genetic data from FIV_{pco} LTR sequences have revealed that both the glucocorticoid receptor (GR) and the pituitary transcription factor 1 (Pit-1) response element are differentially encoded with the LTR between FIV_{pco} viral lineages. GR is a member of a family of steroid receptors that bind glucocorticoid hormones (GCs) such as cortisol and DXM. GCs regulate physiological responses by binding to and modulating the transcriptional activity of the GR (Picard et al., 1990). Alternatively, expression levels of Pit-1 have been shown to increase in response to other hormones inplicated in sexual maturation such as growth hormone (GH) and prolactin (PRL) (Gonzalez-Parra et al., 1998). Therefore, these four steroids, cortisol, DXM, GH and PRL may be appropriate hormones to begin an initial investigation of their effects on FIV_{pco} viral replication.

The level of viral replication in infected cougar PBMC can be measured through a relative real-time PCR assay, which is able to measure changes in target mRNA levels. Relative real-time PCR quantifies mRNA levels of a target gene, in this case possibly *orf-A*, and evaluates *orf-A* expression levels against expression levels of a gene known to remain constant during the cell cycle, for example glyceraldehyde-3-phosphate

dehydrogenase (GAPDH). Cougar PBMC, infected with different viral isolates could be treated with steroid hormones and the level of viral replication can be assayed over a period of time. Additionally FIV_{pco} proviral loads can be quantified during steroid treatment to understand whether proviral loads change with different hormone treatments. Since proviral loads from both the black and gray lineages increase over time, one can hypothesize that PBMC infected with these two viral lineages may increase viral replication and possibly increase proviral loads over the course of hormone treatment. If this is indeed the case then a separate study could investigate the physical interactions of binding the hormone receptor to the LTR of FIV_{pco}.

References

Armstrong, W., Calabrese, L. & Taege, A. J. (2005). HIV update 2005: origins, issues, prospects, and complications. *Cleve Clin J Med* **72**, 73-8.

Beer, B., Scherer, J., zur Megede, J., Norley, S., Baier, M. & Kurth, R. (1996). Lack of dichotomy between virus load of peripheral blood and lymph nodes during long-term simian immunodeficiency virus infection of African green monkeys. *Virology* **219**, 367-75.

Bendinelli, M., Pistello, M., Lombardi, S., Poli, A., Garzelli, C., Matteucci, D., Ceccherini-Nelli, L., Malvaldi, G. & Tozzini, F. (1995). Feline immunodeficiency virus: an interesting model for AIDS studies and an important cat pathogen. *Clin Microbiol Rev* **8**, 87-112.

Biek, R., Rodrigo, A. G., Holley, D., Drummond, A., Anderson, C. R., Jr., Ross, H. A. & Poss, M. (2003). Epidemiology, genetic diversity, and evolution of endemic feline immunodeficiency virus in a population of wild cougars. *J Virol* **77**, 9578-89.

Broussard, S. R., Staprans, S. I., White, R., Whitehead, E. M., Feinberg, M. B. & Allan, J. S. (2001). Simian immunodeficiency virus replicates to high levels in naturally infected African green monkeys without inducing immunologic or neurologic disease. *J Virol* **75**, 2262-75.

Brown, E. W., Yuhki, N., Packer, C. & O'Brien, S. J. (1994). A lion lentivirus related to feline immunodeficiency virus: epidemiologic and phylogenetic aspects. *J Virol* **68**, 5953-68.

Burkhard, M. J. & Dean, G. A. (2003). Transmission and immunopathogenesis of FIV in cats as a model for HIV. *Curr HIV Res* **1**, 15-29.

Burkhard, M. J., Obert, L. A., O'Neil, L. L., Diehl, L. J. & Hoover, E. A. (1997). Mucosal transmission of cell-associated and cell-free feline immunodeficiency virus. *AIDS Res Hum Retroviruses* **13**, 347-55.

Cammarota, G., Da Prato, L., Nicoletti, E., Matteucci, D., Bendinelli, M. & Pistello, M. (1996). Quantitation of feline immunodeficiency proviruses in doubly infected cats using competitive PCR and a fluorescence-based RFLP. *J Virol Methods* **62**, 21-31.

Carpenter, M. A., Brown, E. W., Culver, M., Johnson, W. E., Pecon-Slattery, J., Brousset, D. & O'Brien, S. J. (1996). Genetic and phylogenetic divergence of feline immunodeficiency virus in the puma (Puma concolor). *J Virol* **70**, 6682-93.

Carpenter, M. A. & O'Brien, S. J. (1995). Coadaptation and immunodeficiency virus: lessons from the Felidae. *Curr Opin Genet Dev* **5**, 739-45.

Cato, A. C., Skroch, P., Weinmann, J., Butkeraitis, P. & Ponta, H. (1988). DNA sequences outside the receptor-binding sites differently modulate the responsiveness of the mouse mammary tumour virus promoter to various steroid hormones. *Embo J* **7**, 1403-10.

Chakrabarti, L. A. (2004). The paradox of simian immunodeficiency virus infection in sooty mangabeys: active viral replication without disease progression. *Front Biosci* **9**, 521-39.

Chakrabarti, L. A., Lewin, S. R., Zhang, L., Gettie, A., Luckay, A., Martin, L. N., Skulsky, E., Ho, D. D., Cheng-Mayer, C. & Marx, P. A. (2000). Normal T-cell

turnover in sooty mangabeys harboring active simian immunodeficiency virus infection. *J Virol* **74**, 1209-23.

Chatterji, U., de Parseval, A. & Elder, J. H. (2002). Feline immunodeficiency virus OrfA is distinct from other lentivirus transactivators. *J Virol* **76**, 9624-34.

Clementi, M., Bagnarelli, P., Manzin, A. & Menzo, S. (1994). Competitive polymerase chain reaction and analysis of viral activity at the molecular level. *Genet Anal Tech Appl* **11**, 1-6.

Damond, F., Descamps, D., Farfara, I., Telles, J. N., Puyeo, S., Campa, P., Lepretre, A., Matheron, S., Brun-Vezinet, F. & Simon, F. (2001). Quantification of proviral load of human immunodeficiency virus type 2 subtypes A and B using real-time PCR. *J Clin Microbiol* **39**, 4264-8.

de Parseval, A., Chatterji, U., Sun, P. & Elder, J. H. (2004a). Feline immunodeficiency virus targets activated CD4+ T cells by using CD134 as a binding receptor. *Proc Natl Acad Sci U S A* **101**, 13044-9.

de Parseval, A., Ngo, S., Sun, P. & Elder, J. H. (2004b). Factors that increase the effective concentration of CXCR4 dictate feline immunodeficiency virus tropism and kinetics of replication. *J Virol* **78**, 9132-43.

Desire, N., Dehee, A., Schneider, V., Jacomet, C., Goujon, C., Girard, P. M., Rozenbaum, W. & Nicolas, J. C. (2001). Quantification of human immunodeficiency virus type 1 proviral load by a TaqMan real-time PCR assay. *J Clin Microbiol* **39**, 1303-10.

Dickover, R. E., Donovan, R. M., Goldstein, E., Cohen, S. H., Bolton, V., Huth, R. G., Liu, G. Z. & Carlson, J. R. (1992). Decreases in unintegrated HIV DNA are associated with antiretroviral therapy in AIDS patients. *J Acquir Immune Defic Syndr* **5**, 31-6.

Diehl, L. J., Mathiason-DuBard, C. K., O'Neil, L. L. & Hoover, E. A. (1995). Longitudinal assessment of feline immunodeficiency virus kinetics in plasma by use of a quantitative competitive reverse transcriptase PCR. *J Virol* **69**, 2328-32.

Diehl, L. J., Mathiason-Dubard, C. K., O'Neil, L. L. & Hoover, E. A. (1996). Plasma viral RNA load predicts disease progression in accelerated feline immunodeficiency virus infection. *J Virol* **70**, 2503-7.

Fauci, A. S., Pantaleo, G., Stanley, S. & Weissman, D. (1996). Immunopathogenic mechanisms of HIV infection. *Ann Intern Med* **124**, 654-63.

Gibellini, D., Vitone, F., Schiavone, P., Ponti, C., La Placa, M. & Re, M. C. (2004). Quantitative detection of human immunodeficiency virus type 1 (HIV-1) proviral DNA in peripheral blood mononuclear cells by SYBR green real-time PCR technique. *J Clin Virol* **29**, 282-9.

Goldstein, S., Ourmanov, I., Brown, C. R., Beer, B. E., Elkins, W. R., Plishka, R., Buckler-White, A. & Hirsch, V. M. (2000). Wide range of viral load in healthy african green monkeys naturally infected with simian immunodeficiency virus. *J Virol* **74**, 11744-53.

Gonzalez-Parra, S., Argente, J., Garcia-Segura, L. M. & Chowen, J. A. (1998). Cellular composition of the adult rat anterior pituitary is influenced by the neonatal sex steroid environment. *Neuroendocrinology* **68**, 152-62.

Goto, Y., Nishimura, Y., Baba, K., Mizuno, T., Endo, Y., Masuda, K., Ohno, K. & Tsujimoto, H. (2002). Association of plasma viral RNA load with prognosis in cats naturally infected with feline immunodeficiency virus. *J Virol* **76**, 10079-83.

Gueye, A., Diop, O. M., Ploquin, M. J., Kornfeld, C., Faye, A., Cumont, M. C., Hurtrel, B., Barre-Sinoussi, F. & Muller-Trutwin, M. C. (2004). Viral load in tissues during the early and chronic phase of non-pathogenic SIVagm infection. *J Med Primatol* **33**, 83-97.

Gupta, P., Kingsley, L., Armstrong, J., Ding, M., Cottrill, M. & Rinaldo, C. (1993). Enhanced expression of human immunodeficiency virus type 1 correlates with development of AIDS. *Virology* **196**, 586-95.

Haase, A. T. (1999). Population biology of HIV-1 infection: viral and CD4+ T cell demographics and dynamics in lymphatic tissues. *Annu Rev Immunol* **17**, 625-56.

Ho, D. D. (1997). Perspectives series: host/pathogen interactions. Dynamics of HIV-1 replication in vivo. *J Clin Invest* **99**, 2565-7.

Holzammer, S., Holznagel, E., Kaul, A., Kurth, R. & Norley, S. (2001). High virus loads in naturally and experimentally SIVagm-infected African green monkeys. *Virology* **283**, 324-31.

Hufert, F. T., van Lunzen, J., Janossy, G., Bertram, S., Schmitz, J., Haller, O., Racz, P. & von Laer, D. (1997). Germinal centre CD4+ T cells are an important site of HIV replication in vivo. *Aids* **11**, 849-57.

Inoshima, Y., Miyazawa, T. & Mikami, T. (1998). In vivo functions of the auxiliary genes and regulatory elements of feline immunodeficiency virus. *Vet Microbiol* **60**, 141-53.

Klein, D., Janda, P., Steinborn, R., Muller, M., Salmons, B. & Gunzburg, W. H. (1999). Proviral load determination of different feline immunodeficiency virus isolates using real-time polymerase chain reaction: influence of mismatches on quantification. *Electrophoresis* **20**, 291-9.

Kulkosky, J. & Pomerantz, R. J. (2002). Approaching eradication of highly active antiretroviral therapy-persistent human immunodeficiency virus type 1 reservoirs with immune activation therapy. *Clin Infect Dis* **35**, 1520-6.

Laurence, J., Sellers, M. B. & Sikder, S. K. (1989). Effect of glucocorticoids on chronic human immunodeficiency virus (HIV) infection and HIV promoter-mediated transcription. *Blood* **74**, 291-7.

Leitner, T. & Albert, J. (1999). The molecular clock of HIV-1 unveiled through analysis of a known transmission history. *Proc Natl Acad Sci U S A* **96**, 10752-7.

Leutenegger, C. M., Klein, D., Hofmann-Lehmann, R., Mislin, C., Hummel, U., Boni, J., Boretti, F., Guenzburg, W. H. & Lutz, H. (1999). Rapid feline immunodeficiency virus provirus quantitation by polymerase chain reaction using the TaqMan fluorogenic real-time detection system. *J Virol Methods* **78**, 105-16.

Ligne, M. (1843). Memoire et observations sur une maladie de sang, connue sous le nom d'anhemie hydrohemie, cachexie asquise du cheval. *Rec. Med. Vet. Ec. Alfort* **1843**, 30-44.

Lowenstine, L. J., Pedersen, N. C., Higgins, J., Pallis, K. C., Uyeda, A., Marx, P., Lerche, N. W., Munn, R. J. & Gardner, M. B. (1986). Seroepidemiologic survey of captive Old-World primates for antibodies to human and simian retroviruses, and

isolation of a lentivirus from sooty mangabeys (Cercocebus atys). *Int J Cancer* **38**, 563-74.

Mellors, J. W., Rinaldo, C. R., Jr., Gupta, P., White, R. M., Todd, J. A. & Kingsley, L. A. (1996). Prognosis in HIV-1 infection predicted by the quantity of virus in plasma. *Science* **272**, 1167-70.

Miksicek, R., Heber, A., Schmid, W., Danesch, U., Posseckert, G., Beato, M. & Schutz, G. (1986). Glucocorticoid responsiveness of the transcriptional enhancer of Moloney murine sarcoma virus. *Cell* **46**, 283-90.

Miller, R. J., Cairns, J. S., Bridges, S. & Sarver, N. (2000). Human immunodeficiency virus and AIDS: insights from animal lentiviruses. *J Virol* **74**, 7187-95.

Mitra, D., Sikder, S. & Laurence, J. (1993). Inhibition of tat-activated, HIV-1 long terminal repeat-mediated gene expression by glucocorticoids. *AIDS Res Hum Retroviruses* **9**, 1055-6.

Muller, M. C. & Barre-Sinoussi, F. (2003). SIVagm: genetic and biological features associated with replication. *Front Biosci* **8**, d1170-85.

Muller-Trutwin, M. C., Corbet, S., Tavares, M. D., Herve, V. M., Nerrienet, E., Georges-Courbot, M. C., Saurin, W., Sonigo, P. & Barre-Sinoussi, F. (1996). The evolutionary rate of nonpathogenic simian immunodeficiency virus (SIVagm) is in agreement with a rapid and continuous replication in vivo. *Virology* **223**, 89-102.

Niesters, H. G. (2001). Quantitation of viral load using real-time amplification techniques. *Methods* **25**, 419-29.

Niesters, H. G. (2002). Clinical virology in real time. *J Clin Virol* **25 Suppl 3**, S3-12.

Olmsted, R. A., Langley, R., Roelke, M. E., Goeken, R. M., Adger-Johnson, D., Goff, J. P., Albert, J. P., Packer, C., Laurenson, M. K. & Caro, T. M. (1992). Worldwide prevalence of lentivirus infection in wild feline species: epidemiologic and phylogenetic aspects. *J Virol* **66**, 6008-18.

Orlando, C., Pinzani, P. & Pazzagli, M. (1998). Developments in quantitative PCR. *Clin Chem Lab Med* **36**, 255-69.

Pedersen, N. C., Ho, E. W., Brown, M. L. & Yamamoto, J. K. (1987). Isolation of a T-lymphotropic virus from domestic cats with an immunodeficiency-like syndrome. *Science* **235**, 790-3.

Pedersen, N. C., Leutenegger, C. M., Woo, J. & Higgins, J. (2001). Virulence differences between two field isolates of feline immunodeficiency virus (FIV-APetaluma and FIV-CPGammar) in young adult specific pathogen free cats. *Vet Immunol Immunopathol* **79**, 53-67.

Perelson, A. S., Neumann, A. U., Markowitz, M., Leonard, J. M. & Ho, D. D. (1996). HIV-1 dynamics in vivo: virion clearance rate, infected cell life-span, and viral generation time. *Science* **271**, 1582-6.

Piatak, M., Jr., Saag, M. S., Yang, L. C., Clark, S. J., Kappes, J. C., Luk, K. C., Hahn, B. H., Shaw, G. M. & Lifson, J. D. (1993a). Determination of plasma viral load in HIV-1 infection by quantitative competitive polymerase chain reaction. *Aids* **7 Suppl 2**, S65-71.

Piatak, M., Jr., Yang, L. C., Luk, K. C., Lifson, J. D., Saag, M. S., Clark, S. J., Kappes, J. C., Hahn, B. H. & Shaw, G. M. (1993b). Viral dynamics in primary HIV-1 infection. *Lancet* **341**, 1099.

Picard, D., Kumar, V., Chambon, P. & Yamamoto, K. R. (1990). Signal transduction by steroid hormones: nuclear localization is differentially regulated in estrogen and glucocorticoid receptors. *Cell Regul* **1**, 291-9.

Pistello, M., Menzo, S., Giorgi, M., Da Prato, L., Cammarota, G., Clementi, M. & Bendinelli, M. (1994). Competitive polymerase chain reaction for quantitating feline immunodeficiency virus load in infected cat tissues. *Mol Cell Probes* **8**, 229-34.

Posada, D. & Crandall, K. A. (1998). MODELTEST: testing the model of DNA substitution. *Bioinformatics* **14**, 817-8.

Poss, M., Holley, D. C., Biek, R., Cox, H. & Gerdes, J. (2004). Development of a homology model for clade A human immunodeficiency virus type 1 gp120 to localize temporal substitutions arising in recently infected women. *J Gen Virol* **85**, 1479-84.

Rey-Cuille, M. A., Berthier, J. L., Bomsel-Demontoy, M. C., Chaduc, Y., Montagnier, L., Hovanessian, A. G. & Chakrabarti, L. A. (1998). Simian immunodeficiency virus replicates to high levels in sooty mangabeys without inducing disease. *J Virol* **72**, 3872-86.

Rose, K. M., Marin, M., Kozak, S. L. & Kabat, D. (2004). The viral infectivity factor (Vif) of HIV-1 unveiled. *Trends Mol Med* **10**, 291-7.

Sambrook, J., Fritsch, E.F. and T. Maniatis (1989). Molecular Cloning. Plainview, NY: Cold Springs Harbor Laboratory Press.

Shankarappa, R., Margolick, J. B., Gange, S. J., Rodrigo, A. G., Upchurch, D., Farzadegan, H., Gupta, P., Rinaldo, C. R., Learn, G. H., He, X., Huang, X. L. & Mullins, J. I. (1999). Consistent viral evolutionary changes associated with the progression of human immunodeficiency virus type 1 infection. *J Virol* **73**, 10489-502.

Shimojima, M., Miyazawa, T., Ikeda, Y., McMonagle, E. L., Haining, H., Akashi, H., Takeuchi, Y., Hosie, M. J. & Willett, B. J. (2004). Use of CD134 as a primary receptor by the feline immunodeficiency virus. *Science* **303**, 1192-5.

Sigurdsson, B., Grimsson, H. & Palsson, P. A. (1952). Maedi, a chronic, progressive infection of sheep's lungs. *J Infect Dis* **90**, 233-41.

Swofford, D. L. (2002). PAUP* 4.0b10: phylogenetic analysis using parsimony (and other models).

Troyer, J. L., Pecon-Slattery, J., Roelke, M. E., Black, L., Packer, C. & O'Brien, S. J. (2004). Patterns of feline immunodeficiency virus multiple infection and genome divergence in a free-ranging population of African lions. *J Virol* **78**, 3777-91.